NeuroImage 223 (2020) 117354

Contents lists available at ScienceDirect

NeuroImage

journal homepage: www.elsevier.com/locate/neuroimage

Nested oscillations and brain connectivity during sequential stages of feature-based attention

Mattia F. Pagnotta[a,*], David Pascucci[a,b], Gijs Plomp[a]

[a] Perceptual Networks Group, Department of Psychology, University of Fribourg, Fribourg, Switzerland
[b] Laboratory of Psychophysics, Brain Mind Institute, School of Life Sciences, École Polytechnique Fédérale de Lausanne (EPFL), Lausanne, Switzerland

ARTICLE INFO

Keywords:
Selective attention
Brain rhythms
Functional connectivity
Cross-frequency coupling

ABSTRACT

Brain mechanisms of visual selective attention involve both local and network-level activity changes at specific oscillatory rhythms, but their interplay remains poorly explored. Here, we investigate anticipatory and reactive effects of feature-based attention using separate fMRI and EEG recordings, while participants attended to one of two spatially overlapping visual features (motion and orientation). We focused on EEG source analysis of local neuronal rhythms and nested oscillations and on graph analysis of connectivity changes in a network of fMRI-defined regions of interest, and characterized a cascade of attentional effects at multiple spatial scales. We discuss how the results may reconcile several theories of selective attention, by showing how β rhythms support anticipatory information routing through increased network efficiency, while reactive α-band desynchronization patterns and increased α-γ coupling in task-specific sensory areas mediate stimulus-evoked processing of task-relevant signals.

1. Introduction

Visual selective attention enables us to prioritize the processing of behaviorally relevant stimuli while filtering out irrelevant ones. This fundamental function of the human brain is supported by changes in activity patterns that occur at multiple spatial scales, from local neuronal circuits to global interactions between brain regions (Corbetta and Shulman, 2002; Greenberg et al., 2010; Kastner and Ungerleider, 2000; Scolari et al., 2014; Serences and Yantis, 2007). A central role in this distributed brain function is played by specific rhythms that coordinate selective processing both at the level of neuronal ensembles and at the macro-scale of multiple brain regions, determining the enhancement and propagation of attention-related signals or the downregulation of irrelevant activity (Antzoulatos and Miller, 2014; Bonnefond and Jensen, 2015; Buschman et al., 2012; Buzsáki and Draguhn, 2004; Canolty et al., 2007; Haegens et al., 2011a; Kopell et al., 2000; von Stein and Sarnthein, 2000).

A growing body of evidence suggests that distinct neuronal rhythms may serve distinct functional roles in selective attention. Activity around the alpha rhythm (α, 7–14 Hz), for instance, has been widely linked to the prevention or inhibition of task-irrelevant signals (Chelazzi et al., 2019; Foster and Awh, 2019; Van Diepen et al., 2019; but see Noonan et al., 2016; Schroeder et al., 2018). A potential mechanism by which α rhythms would gate selective attention is through the pulsed inhibition of ongoing cortical activity, by providing phasic bursts of inhibition that suppress the functional processing and inter-areal communication in the gamma frequency range (γ, above 30 Hz) (Jensen and Mazaheri, 2010). In support of this, several studies have recently documented an inverse relationship between α-band feedback signaling from attentional control regions and feedforward γ-band activity in sensory cortices, revealing top-down, attention-related α-modulations that interfere with local structures of α-γ phase-amplitude coupling (PAC) in sensory areas (Bonnefond and Jensen, 2015; Haegens et al., 2011b; Mathewson et al., 2011; Mazaheri and Jensen, 2010; Pascucci et al., 2018; Popov et al., 2017). Intermediate beta rhythms (β, 15–30 Hz) have been instead related to the instantiation of distributed task-relevant representations that convey context- and content-specific information (Antzoulatos and Miller, 2016, 2014; Buschman et al., 2012; Richter et al., 2018; Spitzer and Haegens, 2017). At the same time, β-band activity has been also shown to promote feedforward and inter-areal γ-band synchronization (Richter et al., 2017), while preventing interference and irrelevant attentional shifts (Fiebelkorn and Kastner, 2019). Thus, distinct rhythms appear to fulfill separate but complementary roles in selective attention, by differentially modulating local activity, structures of cross-frequency coupling and neuronal communication in large-scale networks.

A further distinction exists as to whether specialized rhythms support the anticipatory (prestimulus) and reactive (poststimulus) components of selective attention. Prestimulus synchronization of α-band

* Corresponding author.
E-mail address: mattia.pagnotta@unifr.ch (M.F. Pagnotta).

https://doi.org/10.1016/j.neuroimage.2020.117354
Received 27 March 2020; Received in revised form 10 August 2020; Accepted 5 September 2020
Available online 9 September 2020

activity has been mostly described in relation to anticipatory, proactive mechanisms to filter out irrelevant features and locations (Foxe and Snyder, 2011; Kelly et al., 2006; Oliveira et al., 2014; Snyder and Foxe, 2010; Worden et al., 2000; but see Noonan et al., 2016), whereas poststimulus, α-band event-related desynchronization (ERD) has been linked to the release from inhibition (Klimesch et al., 2007), which in turn facilitates local and feedforward γ-band activity conveying task-relevant signals (Bonnefond et al., 2017; Pascucci et al., 2018; Popov et al., 2017). Conversely, poststimulus increases of α-band activity may represent reactive suppression and the return to inhibitory states that prevent task-irrelevant processing (Pascucci et al., 2018). In a similar vein, increases of β-band activity have also been found in preparatory stages of processing (Schneider and Rose, 2016), as top-down modulatory signals that relay task-specific behavioral context (Richter et al., 2018), or in more reactive stages as feedback control mechanisms that facilitate the bottom-up communication of attended stimuli (Bastos et al., 2015). Crucially, most of these phenomena have been investigated separately and the exact nature of their interplay, as well as the complexity of local and large-scale neuronal dynamics involved in selective attention, remains poorly understood.

In the present work, we leveraged different spatial scales of neuronal activity to characterize the temporal dynamics of local and network-level changes during anticipatory and reactive stages of selective attention. At the local level, we focused on neuronal rhythms modulations and on the phenomenon of nested oscillations (Bonnefond et al., 2017). At the network level, we exploited frequency-resolved measures of directed connectivity among distributed attentional and sensory areas, with the goal to assess the role of distinct rhythms in facilitating network-level communication to convey relevant signals, or preventing/filtering out irrelevant ones. Most previous studies on visual attention have investigated local neurophysiological changes and whole-brain connectivity separately (for reviews, see Carrasco, 2011; Scolari et al., 2014). However, local and network changes are highly interdependent because within-area activity co-determines the functional interactions with other areas. Likewise, the interactions with other areas are what shapes local activity. Taking both local and network activities into account is especially pertinent for visual selective attention since it involves preferential processing of features through coordinated activity in a distributed network of areas (Buschman and Kastner, 2015). Local activity changes in distinct frequency bands are thought to reflect specific mechanisms for the processing or inhibition of stimulus features (for review, see Buzsáki, 2006), while network interactions are needed for cognitive tasks. Specifically, mechanisms of large-scale network synchronization are thought to establish information routing of behaviorally relevant information between neuronal groups, through distinct frequency channels of communication (Bastos et al., 2015; Fries, 2015). Here, we therefore investigated both the local activity changes and network reorganization resulting from feature-based selective attention.

In the anticipatory stage, we expected attention-induced local and network-level changes in the α and β-band. Alpha-band changes in preparatory stages have been shown to downregulate irrelevant activity and proactively filter out task-irrelevant signals (Chelazzi et al., 2019; Foster and Awh, 2019; Snyder and Foxe, 2010), while β-band changes are thought to reflect the control of endogenous content reactivation of task-relevant information (Spitzer and Haegens, 2017). We thus expected α-band power increases in task-specific sensory areas in anticipation of task-irrelevant (unattended) stimuli, accompanied by facilitation of network-level communication in the α-band to convey gating signaling to these areas; vice versa, locally increased β power and enhanced information routing in the β-band were expected in anticipation of task-relevant (attended) stimuli to endogenously reactivate content-specific relevant representations. As for the reactive stage of selective attention, a recent study using an orientation discrimination task showed that attention-induced α-band ERD was accompanied by increase in α-γ PAC in early visual areas (Pascucci et al., 2018), which may reflect an enhancement in sensory processing of relevant exogenous signals of attended stimuli (Bonnefond and Jensen, 2015; Jensen and Mazaheri, 2010). Here, we expected similar reactive effects to selectively occur in sensory cortices that preferentially encode the attended feature, together with a dynamic reorganization of frequency-specific inter-areal interactions in the α and γ-band. The feature-based specificity of attention may emerge from these more local, selective coupling mechanisms in functionally specialized regions, while general effects of stimulus relevance may involve more global phenomena, characterized by dynamic changes in the network organization of functional interactions between distributed cortical areas. With regards to network changes, previous work has shown that γ-band interactions support information routing of attended sensory representations, while interactions in the α and β-band would mediate the suppression of task-irrelevant information and provide endogenous control, respectively (Fiebelkorn and Kastner, 2019; Fries, 2015; Jensen and Mazaheri, 2010; Spitzer and Haegens, 2017). During the reactive stage of processing of attended stimuli, we therefore expected changes in local and global network efficiency characterized by i) facilitation of communication in the γ-band and ii) impediment in the α and β-band.

To test our hypotheses, we acquired separate EEG and fMRI recordings while human participants were performing basic visual tasks under different feature-based attention conditions. We presented two spatially overlapping features (Baldauf and Desimone, 2014), motion and orientation, and we directed participant's attention toward one of them in separate blocks, probing both anticipatory and reactive feature-specific attentional responses. We used EEG for its high temporal resolution and ability to resolve spectral components. Since analyses in EEG sensor-space do not allow meaningful interpretation in terms of underlying interacting cortical areas (Brunner et al., 2016; Van de Steen et al., 2016), we employed a source reconstruction technique using individual head models (Pascual-Marqui et al., 2017; Rubega et al., 2019; Van Veen et al., 1997). Source-reconstructed EEG signals were extracted from 22 cortical regions of interest (ROIs), as identified using fMRI contrasts from the same participants. We adopted an fMRI-based approach to localize attention-induced effects and define ROIs. This takes into account the specific characteristics of our experimental design and the physical properties of the visual stimuli employed, and can be expected to be more accurate than using a priori selections based on previous studies, where paradigm and stimuli characteristics may differ from those used here. This approach allowed us to identify known attentional areas in frontal and parietal cortices (Corbetta and Shulman, 2002), as well as additional sensory areas that may be specific for the paradigm and visual features used in this study (Ahlfors et al., 1999; Bosking et al., 1997; Dupont et al., 1998; Koelewijn et al., 2011; Schoenfeld et al., 2007; Simoncelli and Olshausen, 2001).

Analyses on source-reconstructed EEG signals enabled us to characterize the temporal dynamics of i) local neuronal rhythms, ii) nested oscillations, and iii) whole-brain connectivity, as a function of attentional condition. Local rhythmic modulations were quantified using Morlet wavelet transform (Torrence and Compo, 1998), while nested oscillations were assessed using measures of PAC (Lachaux et al., 1999; Penny et al., 2008). A time-varying connectivity analysis was employed to derive frequency-resolved measures of directed connectivity (Baccalá and Sameshima, 2014; Pascucci et al., 2020; Takahashi et al., 2010), and we used graph theoretical analysis to summarize the topological organization of large-scale functional networks in the time and frequency domain. Our brain, like many other natural networks, is characterized by a network organization that favors both functional segregation and integration, which are respectively the ability for specialized processing within densely interconnected neuronal groups and the ability to quickly access and combine specialized information from these distributed groups across areas (Rubinov and Sporns, 2010). These were traditionally quantified using network measures like the mean clustering coefficient and characteristic path length, such that high clustering and short characteristic path length characterize networks that are simultaneously highly segregated and integrated (Watts and Strogatz, 1998).

More recent measures of segregation and integration are the local and global network efficiency (Latora and Marchiori, 2001). These quantify the levels of functional integration within subgraphs of interconnected brain regions and globally in the entire network respectively, and have the interpretational advantage that higher efficiency values indicate more integration, locally or globally. Simultaneously increased local and global efficiency would represent enhanced large-scale network communication, facilitating information routing, while decreased levels would represent reduced communication at certain frequencies and time points. Although it seems reasonable to expect that network topology dynamically changes during stimulus processing (Ju and Bassett, 2020), its dynamics and relevance for attentional processing remain unexplored.

The analyses of neuronal rhythms and nested oscillations were expected to characterize the dynamic modulations of local cortical computations induced by attention in specialized sensory areas, while the graph analysis was expected to shed light on how selective attention flexibly and dynamically reorganizes functional network interactions to render such specialized information more widely accessible across cortical regions, supporting the preferential processing of endogenously- or exogenously-driven relevant signals in widespread circuits. Our results revealed a cascade of attentional effects at multiple spatial scales, from anticipatory β-band connectivity changes to facilitate network-level communication, to distinct local and global poststimulus dynamics initiated by α-band desynchronization.

2. Methods

2.1. Participants

Twenty healthy human participants (13 female; all right-handed; ages 19–34 y, M = 23.25, SD=4.15) with normal or corrected-to-normal vision (visual acuity across participants 1.10–1.63, M = 1.40, SD=0.19; Freiburg visual acuity test (Bach, 1996)) took part in the study for monetary compensation (20.– CHF/hour). The study was performed in accordance with the Declaration of Helsinki on "Medical Research Involving Human Subjects" and after approval by the responsible ethics committee (Commission cantonale d'éthique de la recherche sur l'être humain, CER-VD). Written informed consent was obtained from each participant prior to the experimental sessions. Data from one participant (male, age = 22) were excluded because of excessive artifacts in the EEG. These consisted of irregular drifts over several electrodes (due to inappropriate fitting of the headcap), as signaled by electrode offset outside the acceptable range for legitimate recordings (within +/- 25 mV).

2.2. Experimental design

Visual stimuli were Random Dot Kinematograms (RDK: 10° field-size, 1200 dots, 0.2° dot-size, infinite dot-life, and 4°/s dot-speed), that were contrast-modulated through a Gaussian-windowed sinusoidal grating (Gabor: 6° width at 3 SDs, and 0.5 cycles/° spatial frequency), such that the Gabor determined the visible region of the RDK and its spatial pattern of contrast (Fig. 1). The orientation of the Gabor ranged between 45° and −45° off-vertical, and phase varied randomly at every trial. In the RDK, a subset of dots moved coherently either towards left or towards right (signal-dots), while the remaining dots moved with random walks (noise-dots), in such a way that their direction varied at every frame but their speed was kept constant. Stimuli were presented on a gray background for 300 ms always at the same spatial location, around a central fixation spot that was constantly on the screen (0.2° size, and (0,0,160) color in RGB digital 8-bit notation). The inter-trial interval (ITI) was randomly varied between 800 and 1000 ms. The generation and presentation of the visual stimuli was performed using a combination of in-house Python codes and PsychoPy Builder (Peirce et al., 2019).

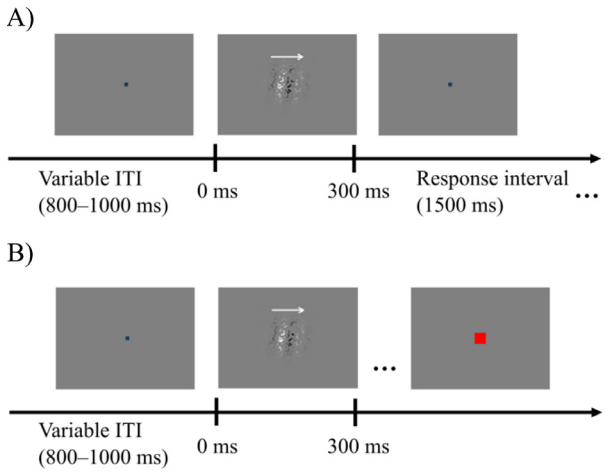

Fig. 1. Experimental paradigm. Schematic representation of the trial structure for A) Attended (motion or orientation discrimination) and B) Unattended (detection of color changes in the fixation spot) conditions. The white arrows on top of the visual stimuli indicate the direction of coherent motion and were not present during the experiment. The red fixation spot is enlarged for illustrative purpose, but it did not change size during color changes.

The study consisted of three separate experimental sessions: one behavioral (approx. 45 min), one EEG (approx. 60 min), and one session of fMRI (approx. 45 min). In all sessions, the participants were asked to performed different tasks on the same type of visual stimuli. The behavioral session comprised two different tasks in separate blocks (100 trials), requiring a two-choice response. At the beginning of each block, participants were either instructed to report the perceived motion direction in the RDK (left vs. right, motion discrimination task), or the off-vertical tilt of the Gabor (left vs. right, orientation discrimination task), by pressing the corresponding key on a keyboard. The aim of the behavioral session was to determine individual thresholds for coherent motion and orientation discrimination, in order to level performance for the two tasks in the EEG and fMRI sessions, keeping accuracy at 82% of correct responses for both tasks. Thresholds were estimated using the adaptive staircase procedure QUEST (Watson and Pelli, 1983) as implemented in PsychoPy, which measures psychophysical thresholds using a Weibull psychometric function, where desired correct performance of 82% is typically used (see, e.g., Pascucci et al., 2018). We used starting values of 60% for signal-dots and 4° for angle of orientation, while the task-irrelevant feature was kept constant during the staircase procedure (40% of signal-dots in the orientation discrimination task and ±3° off-vertical in the motion discrimination task). This allowed to obtain individual discrimination thresholds at the same level of accuracy across participants, both for the motion discrimination task (signal-dots percentages 10.61–89.82, M = 44.50, SD=29.09) and for the orientation discrimination task (angles of orientation 1.53°–4.30°, M = 2.45°, SD=0.72°). Individually calibrated values were used to define stimuli in the subsequent EEG and fMRI sessions.

During neuroimaging sessions, participants also performed an additional control task, where they had to report sporadic color changes in the fixation spot lasting 200 ms (from dark blue to red, 30% of trials; Fig. 1B) by pressing a response button. To ensure that the timing of these color changes was unpredictable, we presented them at any time during the trial, randomly. Trials in which the color change overlapped with visual stimuli appearance were excluded from the successive analyses. This design resulted in two conditions in which the RDK was task-relevant (motion and orientation discrimination) and one condition where it was task-irrelevant (color change detection). We refer to these different task conditions as Attended (Attended-motion and Attended-orientation) and Unattended, indicating the type of attentional processing required for the visual stimuli. Task order was counterbal-

anced across participants in each of the three experimental sessions. Participants had a limited time to respond (1500 ms), after which the response for that trial was considered incorrect. The EEG session consisted of 160 trials for each task condition, which were divided in 4 blocks (40 trials per block). Small breaks were offered between blocks. The fMRI session followed a similar block structure, but with less trials (48 trials for each task condition). Here, a fixed 12 s break was presented after each block following the instruction to "REST" (Rest period), with the exception of the last Rest period that lasted 60 s. The aim of the fMRI session was to identify regions of interest (ROIs) for source-space EEG analyses (see Section 2.4 and Supplementary material).

2.3. EEG data acquisition and preprocessing

EEG recordings were collected at the Department of Psychology, University of Fribourg. During the EEG session, participants were sitting inside a dark, electromagnetic shielded room, with their head leaning on a chinrest positioned at 71 cm from a VIEWPixx /EEG^{TM} (VPixx Technologies Inc., Saint-Bruno, CA) LCD monitor (24 inches diagonal size, 1920×1080 resolution, 100 cd/m^2 luminance, 120 Hz refresh rate, 1 ms pixel response time). A 2-button RESPONSEPixx response box (VPixx Technologies Inc.) was plugged into the monitor and used by the participants during the visual tasks. EEG data were acquired using a 128-channel ActiveTwo EEG system (Biosemi, Amsterdam, NL). Data acquisition was performed at a sampling rate of 1024 Hz, and signals were referenced to the Common Mode Sense (CMS) active electrode, which together with the Driven Right Leg (DRL) passive electrode formed a feedback loop in the system. This CMS/DRL loop allow to drive the common-mode voltage as close as possible to the ADC reference voltage in the AD-box, and to obtain an extra 40 dB common-mode rejection ratio at 50 Hz, when compared with using normal ground electrodes with same impedance. At the end of the EEG session, the 3D coordinates of the positions of the electrodes were localized for each participant using an ELPOS system (Zebris Medical GmbH, Isny im Allgäu, DE). These individual electrodes' positions were used for EEG source reconstruction procedure (see Section 2.4).

EEG preprocessing was performed using a combination of EEGLAB (Delorme et al., 2011; Delorme and Makeig, 2004), its plugins, and in-house scripts implemented in MATLAB (The MathWorks Inc., Natick, USA). Data were first downsampled to 500 Hz using an anti-aliasing filter with 125 Hz cutoff frequency and 50 Hz transition bandwidth. Afterwards, the data were detrended using high-pass filtering (1 Hz low-frequency cutoff), as implemented in the PREP plugin (Bigdely-Shamlo et al., 2015). Line noise and its harmonics were reduced using the adaptive filtering technique implemented in the EEGLAB plugin CleanLine (https://www.nitrc.org/projects/cleanline), which allows identifying and removing significant sinusoidal artifacts. Epochs were extracted using the time window −1500–1000 ms around stimulus onset. Noisy EEG channels were identified by visual inspection and removed before proceeding to the subsequent preprocessing steps (number of removed channels across participants 12–21, M = 15.85, SD=2.64). Epochs contaminated by noise artifacts were also rejected by visual inspection, and the same was done for those with eye blinks occurring within 500 ms from stimulus onset (−500–500 ms window) (percentage of rejected epochs across participants 12.50–38.95%, M = 23.01, SD=7.49). Decomposition of EEG data by independent component analysis (ICA) was performed using the FastICA algorithm (Hyvärinen and Oja, 2000). ICA components identified as eye artifacts or muscular activity artifacts were removed from the data (number of removed components across participants 5–23, M = 10.30, SD=4.09). As final preprocessing steps, noisy EEG channels were interpolated using a spherical spline interpolation (Perrin et al., 1989); then, the signals were re-referenced to the common average reference (Lehmann and Skrandies, 1980). Trials with incorrect responses were excluded from successive analyses. Moreover, because the functional connectivity analysis (see Section 2.7) can be sensitive to the amount of trials (Astolfi et al., 2008; Toppi et al., 2012), and consequently an imbalance of trials between task conditions may create spurious differences from comparing them, the amount of trials across task conditions was balanced within-subjects (number of trials per task condition across participants 74–127, M = 103.5, SD=15.3). This was accomplished by randomly removing trials in each condition to match the minimum amount across the three task conditions at within-subject level (maximum percentage of trials removed per task condition across participants 0.63–13.75%, M = 6.3%, SD=4.7%).

2.4. EEG source reconstruction

Source reconstruction techniques enable to estimate and localize the EEG sources of brain electrical activity, by solving first a forward problem and then an inverse problem (Michel et al., 2004). For the forward problem, the volume conduction model of each participant was constructed using a boundary element method (BEM) (Hamalainen and Sarvas, 1989), which employed the information about boarder surfaces between three different tissue-types: scalp, skull and brain. These surfaces were obtained from a segmentation procedure of the individual-participant anatomical MRI, using a Gaussian kernel for smoothing (5 voxels FWHM). The participant-specific 3D electrode coordinates were aligned to the head model of the same participant using an interactive re-alignment procedure, followed by a projection of electrodes onto the head surface. For group analyses on source-reconstructed EEG data, we employed a template grid based on Montreal Neurological Institute and Hospital (MNI) template anatomical MRI to define the solution points. The template comprised 1725 source-points (equivalent current dipoles) with 10 mm spacing, and was constrained to be within the cortical gray matter. Individual MRIs were warped to the template, and the inverse of this warping procedure was applied to the template grid. This procedure provided participant-specific grids that were no longer regularly spaced, but that became equivalent across participants in normalized MNI space, facilitating group analysis on source-space. Finally, individual lead field matrices were computed considering an unconstrained-orientation forward operator, i.e., each solution point was modeled as three orthogonal equivalent current dipoles placed at that location.

To solve the EEG inverse problem, we employed the linearly constrained minimum variance (LCMV) beamformer (Van Veen et al., 1997). The LCMV belongs to the family of spatial filtering methods and its implementation relies on the use on an estimate of the sensor-space covariance matrix, which was here estimated from the time window −500–500 ms around stimulus onset. Source-reconstructed signals were extracted from 22 cortical ROIs using singular value decomposition (SVD), deriving scalar-value time series that best explain the variability in dipole orientations and strengths across trials, for each ROI (for details see Rubega et al., 2019). An automatic procedure starting from the results of an fMRI statistical analysis allowed to identify the 22 ROIs (for details, see Supplementary material): left and right premotor area (PM L and R), left and right middle frontal gyrus (MFG L and R), left and right inferior frontal gyrus (IFG L and R), supplementary motor area (SMA), middle cingulate cortex (MCC), left and right calcarine sulcus (V1 L and R), left cuneus (Cuneus), left and right secondary visual cortex (V2 L and R), left fusiform gyrus (FFG L), left gyrus postcentralis (GPC L), left and right superior parietal lobule (SPL L and R), left and right inferior parietal lobule (IPL L and R), left and right middle temporal area (MTG L and R), right visual cortex V5 (V5 R). As a final step, we used orthogonalization for leakage correction (Pascual-Marqui et al., 2017), on the single trial scalar-valued time series derived using SVD. This orthogonalization approach allowed reducing the detrimental effects on functional connectivity analyses of zero-lag cross-correlations, which are due to instantaneous linear mixing between source-reconstructed signals (source leakage) and are known to produce spurious functional connectivity estimates (Anzolin et al., 2019). All the steps of EEG source reconstruction were implemented using in-house MATLAB codes and routines from

FieldTrip (Oostenveld et al., 2011) (Radboud University, Nijmegen, NL; http://www.ru.nl/neuroimaging/fieldtrip).

2.5. Power spectra

To investigate local brain rhythms modulations depending on whether the stimuli were relevant or not, time-varying power spectra were estimated in the time window −800–800 ms around stimulus onset from the source-reconstructed signals in each ROI. The estimation was performed using a Morlet wavelet transform with central frequency parameter $\omega_0 = 6$, in combination with zero-padding to solve the problem of edge effects (Torrence and Compo, 1998). For each participant and task condition, time-varying spectral estimates were estimated in the frequency range 1–100 Hz using the MATLAB codes made available in Pagnotta et al., 2018a.

To characterize the attentional modulations of neuronal rhythms in the reactive stage of processing (locked to stimulus onset), a cluster-based permutation approach was used to compare time-varying power spectra of Attended and Unattended conditions, over time frames (0–500 ms after stimulus onset) and frequencies (1–100 Hz), and all ROIs (Maris and Oostenveld, 2007). In this and every other analysis using a cluster-based permutation approach to compare Attended and Unattended conditions, we employed the same settings: two-tailed dependent *t*-test ($p<0.05$), 50,000 permutations, and $p<0.05$ for the permutation test. In the two-tailed test, we used the solution that consists of multiplying the *p*-values with a factor of two, prior to thresholding, to distribute alpha level over both tails (http://www.fieldtriptoolbox.org/faq/why_should_i_use_the_cfg.correcttail_option_when_using_statistics_montecarlo/).

To assess neuronal rhythms modulations in the anticipatory stage, a similar analysis was performed on a prestimulus time window of interest (−300–0 ms). We selected this prestimulus window to be as distant from the previous behavioral response as possible, while keeping a large enough window size to consider a central frequency for the phase time series above 4 Hz, for the PAC analysis (see Section 2.6.1). We averaged spectral estimates over the prestimulus window since there was no temporal reference in the anticipatory window, and then compared Attended and Unattended conditions using a cluster-based permutation approach over frequencies (1–100 Hz) and ROIs.

2.6. Local cross-frequency coupling

2.6.1. Anticipatory cross-frequency coupling

Cross-frequency coupling was measured in terms of dependence between phase of low-frequency oscillations and amplitude of high-frequency oscillations, called phase-amplitude coupling or PAC. Among the available types of cross-frequency coupling, we employed the PAC because of its more clear functional role and physiological plausibility (Canolty and Knight, 2010; Voytek et al., 2010). Several approaches have been proposed to measure PAC (Canolty et al., 2006; Martínez-Cancino et al., 2019; Penny et al., 2008; Tort et al., 2010; Voytek et al., 2013). We here employed the modulation index based on GLM (Penny et al., 2008) to calculate within-region PAC, using the toolbox from Martínez-Cancino et al. (2019). Since previous studies reported attention-related modulations of low-frequency activity and PAC (especially α-γ) in sensory areas (Bonnefond and Jensen, 2015; Haegens et al., 2011b; Mathewson et al., 2011; Mazaheri and Jensen, 2010; Pascucci et al., 2018; Popov et al., 2017), our analysis was restricted to the occipito-temporal ROIs: V1 L and R, Cuneus, V2 L and R, FFG L, MTG L and R, and V5 R.

The anticipatory PAC analysis was performed in the window −300–0 ms. The central frequency for the phase time series (f_{PHASE}) ranged from 4 Hz to 30 Hz in 1Hz-steps, and the higher central frequency for the amplitude time series ($f_{AMPLITUDE}$) ranged from 40 Hz to 100 Hz in 2Hz-steps. The bandwidth of the band-pass filters to estimate the phase time series (BW_{PHASE}) and the amplitude time series ($BW_{AMPLITUDE}$) were defined according to the following expressions:

$$\begin{aligned} BW_{PHASE}(Hz) &= \left[f_{PHASE} - 1,\ f_{PHASE} + 1\right] \\ BW_{AMPLITUDE}(Hz) &= \left[f_{AMPLITUDE} - \left(f_{PHASE} + 1\right),\right. \\ &\quad \left. f_{AMPLITUDE} + \left(f_{PHASE} + 1\right)\right] \end{aligned} \quad (1)$$

Filtering was applied to the time window of interest using two buffer windows of 1850 ms, before and after the window. Each buffer window consisted of 600 ms of observed signal and the rest zeros, such that filtering was applied every time to a 4000 ms window. A combination of high-pass and low-pass finite impulse response (FIR) filters was employed to band-pass filter the data in the frequency bands of interest. Next, the Hilbert transform was applied to extract the analytic signals from which instantaneous low-frequency phase and high-frequency amplitude time series were estimated, which allowed computing PAC in the time window of interest using the GLM-based method. This procedure was repeated for every combination of f_{PHASE} and $f_{AMPLITUDE}$, in each trial. Single-trial estimates were averaged to obtain the within-region PAC in the different task conditions.

In each task condition, the presence of local oscillatory nesting was determined by a statistical test using surrogate data (Aru et al., 2015). In this surrogate analysis, PAC estimates were obtained 500 times from surrogate data. Surrogate data were generated using a block-resampling technique where the time series of instantaneous low-frequency phase was separated into 20 segments. The segments were then randomly permuted across time and a new PAC estimate (surrogate) was derived. The statistical significant of each PAC estimate (from actual data) was assessed against the distribution of surrogates, following the approach based on z-scores (alpha level of 0.05) described by Martínez-Cancino et al. (2019).

After surrogate analysis, significant within-region PAC estimates (masked) were compared between Attended and Unattended conditions, using a cluster-based permutation approach over all pairs of f_{PHASE} and $f_{AMPLITUDE}$. The f_{PHASE}–$f_{AMPLITUDE}$ pairs for which $BW_{AMPLITUDE}$ overlapped with BW_{PHASE} were excluded from the analysis. Since strong imbalances in the power spectra between conditions can lead to spurious PAC differences (Aru et al., 2015), a control analysis based on a stratification procedure was used to confirm the between-condition differences in PAC. The control analysis was performed using the *ft_stratify* function from FieldTrip with 1000 iterations (Oostenveld et al., 2011), separately for each ROI that showed significant differences in PAC from the previous cluster-based permutation comparison. At each iteration, this procedure selects subsets of trials from the two conditions with matched distributions of power spectra across trials, for both phase and amplitude frequency bands. Balanced numbers of trials between conditions were maintained during this procedure. The final estimates from this control analysis were obtained as the median across iterations of the power-balanced estimates, and these were compared between Attended and Unattended conditions using the cluster-based permutation.

2.6.2. Reactive α-γ coupling

A measure of stimulus-evoked cross-frequency coupling was computed for each task condition using the instantaneous phase-locking value (PLV) between the low-frequency phase and the phase of amplitude-filtered high-frequency signal (Lachaux et al., 1999; Pascucci et al., 2018). Same as before, the estimation was performed on the subset of 9 occipito-temporal ROIs. Time-varying estimates were obtained at each time frame by averaging the instantaneous contributes across trials. The analysis was performed on the interval 0–500 ms after stimulus onset, using two buffer windows (before/after), each of 1450 ms length (including 300 ms of observed signal). Low-frequency range was defined in the α-band as $f_{PHASE} = 10$ Hz. This value was selected in a data-driven way, based on results obtained by comparing time-varying power spectra (Fig. 4). For the amplitude time series, $f_{AMPLITUDE}$ ranged from 40 Hz to 100 Hz in 2Hz-steps. The bandwidths of the two band-pass filters were chosen using the expressions

in Eq. (1); the procedure of filtering (FIR-based) and analytic signals extraction (using Hilbert transform) was carried out as previously (see Section 2.6.1). The presence of within-region α-γ coupling in each task condition was determined using surrogate analysis (Aru et al., 2015; Martínez-Cancino et al., 2019). A cluster-based permutation approach over time frames and amplitude high-frequencies was then employed to compare significant instantaneous PLV estimates (masked) between Attended and Unattended conditions. Finally, a control analysis based on stratification (1000 iterations) was used to confirm between-condition differences in time-varying α-γ coupling, by selecting at each iteration subsets of trials from the two conditions with matched distributions of power spectra, for both phase and amplitude frequency bands (Aru et al., 2015). The stratification procedure was here performed separately for each time frame.

2.7. Large-scale networks

To estimate the functional interactions among ROIs we used the *information* form of partial directed coherence (iPDC) (Takahashi et al., 2010). The iPDC is based on the notion of Granger-Geweke causality (Geweke, 1984; Granger, 1969), which relies on the concepts of temporal precedence and statistical predictability between simultaneously recorded time-series, extended to the spectral-domain (Seth et al., 2015). Computationally the iPDC is derived from a multivariate autoregressive (MVAR) model with a certain order, which determines the number of past observations included in the model. To derive iPDC estimates the MVAR coefficients are Fourier transformed, appropriately weighted by the noise covariances to overcome the scale-variance problem, and then normalized. This assures that the resulting connectivity estimates are scale-invariant and not affected by local differences in signal power (Baccalá and Sameshima, 2014). The iPDC is a measure of the partialized delayed functional interactions between ROIs, which is able to characterize the interaction directionality between them (directed measure), as well as discerning direct from indirect or mediated paths of connections (directness). More precisely, the iPDC from the j-th time series to the i-th time series is equivalent to the squared coherence between the innovation process associated with i and the partialized version of j, which via appropriate logarithmic expression and integration provides the mutual information rates between these two processes (Baccalá and Sameshima, 2014; Takahashi et al., 2010). In the present study, the iPDC was used as measure of the frequency-specific, directed connections between ROIs, and all connectivity analyses were performed on source-reconstructed time series, because analyses applied on EEG sensor-space time series do not allow any meaningful interpretation in terms of interacting brain sources (Brunner et al., 2016; Van de Steen et al., 2016).

To accommodate the non-stationarity of signals and obtain time-varying functional interactions in our network of 22 ROIs, the iPDC can be derived from a time-varying MVAR (tvMVAR) model of the signals, which can be computed using adaptive algorithms (Arnold et al., 1998; Milde et al., 2010; Pagnotta and Plomp, 2018). This procedure allows obtaining iPDC estimates over frequencies and time frames. For each participant and task condition, time-varying iPDC estimates were computed in the interval −800–800 ms around stimulus onset and in the frequency range 1–100 Hz (in 1Hz-steps), after decimating single-trial data by a factor of two. We performed tvMVAR modeling with the Self-Tuning Optimized Kalman filter (STOK) algorithm (Pascucci et al., 2020), using a percentage of variance explained of 99% for setting the filtering factor threshold (Hansen, 1987). The optimal model order for each participant was selected by first identifying the value that minimized the difference between power spectra obtained from parametric tvMVAR modeling and those obtained using a nonparametric approach based on wavelet transform (see Section 2.5), in each task condition separately, and then selecting the maximum value across task conditions (model orders across participants 11–24, $M = 17.79$, SD=2.94). This approach optimizes model quality within participants and was adopted to best reflect the temporal structure of the recorded data, and avoid choices based on a group estimate, which may be driven by subjects with the poorest data quality.

We employed measures from graph theory to characterize large-scale topological properties of the frequency-specific, directed functional networks in the different task conditions (Rubinov and Sporns, 2010). Each ROI was considered as a node in the graph and two measures were estimated: global efficiency and local efficiency. The network's global efficiency is the average inverse shortest path length and indicates the level of global functional integration in the network (Latora and Marchiori, 2001). The single node's local efficiency is the global efficiency of the local subgraph comprising all its immediate neighbors (Latora and Marchiori, 2001), and the network's local efficiency is computed as average efficiency of all local subgraphs, which represents the level of local integration within subgraphs. High local efficiency suggests functional segregation within the network (Rubinov and Sporns, 2010). Both global efficiency and local efficiency were computed for each participant and task condition from the full matrix of iPDC estimates, i.e., from a fully-connected, weighted and directed adjacency matrix. Subgraphs and nodes' neighbors were thus determined by the interaction strengths: the stronger the connection weight between two nodes, the closer they were (functionally). When we consider global and local efficiency derived from iPDC-based graphs, we can talk about frequency-specific levels of functional integration among ROIs, respectively globally and within subgraphs, for two reasons. First, the iPDC has a clear interpretation in terms of between-processes mutual information rates, providing an association with the notion of information flow (Baccalá and Sameshima, 2014; Takahashi et al., 2010). Second, thanks to its partialization approach, the iPDC provides the directness of functional connections. It is therefore reasonable to characterize the cascades of these direct connections as paths of integration between ROIs, unlike when using classical measures such as cross-correlations and spectral coherence (Rubinov and Sporns, 2010).

To investigate the anticipatory network-level modulations of attention, time-varying iPDC estimates were first averaged over the anticipatory window (−300–0 ms), as for anticipatory power changes (see Section 2.5). Frequency-specific global and local network efficiency were then estimated for each participant and task condition. Finally, each graph measure was separately compared between Attended and Unattended conditions (two-tailed dependent t-test, $p<0.05$, with FDR correction). To assess network-level modulations in the reactive stage, measures of time-varying global efficiency and local efficiency were analyzed in the time window 0–500 ms from the full matrix of time-varying iPDC estimates. A cluster-based permutation approach was used to compare graph measures of Attended and Unattended conditions at each time point (0–500 ms after stimulus onset) and frequency (1–100 Hz). Graph measures were derived using the Brain Connectivity Toolbox (Rubinov and Sporns, 2010) (http://www.brain-connectivity-toolbox.net). All the other steps of the functional connectivity analysis were performed using in-house scripts implemented in MATLAB.

2.8. Data availability

Preprocessed EEG data on sensor-space and source-reconstructed signals are available at https://doi.org/10.17605/OSF.IO/2ZQNT.

3. Results

The behavioral task required the participants to attend visual stimuli presented at central location (Fig. 1A), and to discriminate either the motion direction of signal-dots in the Random Dot Kinematograms (RDK; motion discrimination task), or the off-vertical tilt of the Gabor (orientation discrimination task). These two tasks conditions are named Attended-motion and Attended-orientation, respectively. In each Attended condition, stimuli contained both features (motion and orientation). In a third task condition that served as control, participants were asked to report sporadic color changes in the fixation spot (Fig. 1B),

which rendered the same stimuli irrelevant for the task (Unattended condition), without changing their physical characteristics. We calibrated task-difficulty beforehand (see Methods) and did not observe differences in behavioral performance between the two discrimination tasks. Percentage correct was 89.0% (*SD*=5.2) and 88.6% (*SD*=7.2) for Attended-motion and Attended-orientation respectively (t = 0.19, p = 0.8485), with corresponding reaction times (RTs) of 687.5 ms (*SD*=159.1) and M = 699.5 ms (*SD*=141.0; t ==−0.62, p = 0.5432). In the Unattended control condition, participants correctly detected a color change in the fixation spot in 99.2% of target trials (*SD*=1.4), with RT of 484.4 ms (*SD*=46.6).

3.1. Anticipatory stage: modulations of β-band rhythms

The investigation of the attentional modulations of local neuronal rhythms, like any other analysis presented in this article, was carried out on EEG source-reconstructed signals. We employed EEG source reconstruction techniques based on individual lead-fields to extract the signals from 22 cortical ROIs distributed across the brain (Oostenveld et al., 2011; Pascual-Marqui et al., 2017; Rubega et al., 2019; Van Veen et al., 1997). Time-varying power estimates in each ROI were obtained with the Morlet wavelet transform (Torrence and Compo, 1998).

To assess attention-related neuronal rhythms modulations in the anticipatory stage, time-varying power estimates in each ROI were averaged over the anticipatory window (−300–0 ms) and then compared between Attended and Unattended conditions over frequencies (1–100 Hz) (see Methods). The results showed anticipatory β-band power increases in the Attended conditions compared to Unattended. For the comparison between Attended-motion and Unattended, we found significant power increases in PM L (with p-value for the permutation test p_{perm}<0.01), SPL L (p_{perm}<0.05), FFG L (p_{perm}<0.05), MTG L (p_{perm}<0.05), and in secondary visual cortices V2 L and R (p_{perm}<0.05) (Fig. 2A). Similarly, we found significant power increases in PM L (p_{perm}<0.05), FFG L (p_{perm}<0.001), Cuneus (p_{perm}<0.05), and V2 R (p_{perm}<0.005) from comparing Attended-orientation and Unattended (Fig. 2B). The results show that local anticipatory effects of attention involved increased β-band power, mostly in left prefrontal cortex and some occipito-temporal ROIs, irrespective of the attended feature (motion or orientation).

3.2. Anticipatory stage: increased β-band network efficiency

To characterize whole-brain connectivity changes due to attention, we estimated the frequency-specific directed connections between the 22 ROIs using a multivariate functional connectivity measure, the iPDC (Baccalá and Sameshima, 2014; Takahashi et al., 2010). Time- and frequency-resolved iPDC estimates were derived from tvMVAR modeling using the STOK algorithm (Pascucci et al., 2020). To describe and compare the topological properties of the resulting networks, we used two graph measures: global efficiency and local efficiency (Latora and Marchiori, 2001; Rubinov and Sporns, 2010). Given the ability of the iPDC to characterize both directionality and directness of interareal connections and because of its information-theoretic foundation (Baccalá and Sameshima, 2014; Takahashi et al., 2010), these functional connections can be seen as paths of integration between network nodes (ROIs). The iPDC-derived global efficiency represents the frequency-specific level of global functional integration among all ROIs. Likewise, the local efficiency represents the level of functional integration within subgraphs of neighboring ROIs (functional segregation), defined by strongest functional connections (see Methods).

In the anticipatory window (−300–0 ms), topological network analysis revealed that attention to motion significantly increased both global and local network efficiency in the β-band (network more highly integrated and segregated), with significant differences (p_{FDR}<0.05) in the ranges 18–23 Hz and 17–22 Hz, respectively (Fig. 3A–B). We found analogous increases for the comparison between Attended-orientation and Unattended, where statistically significant differences in the β-band (p_{FDR}<0.05) spanned larger frequency ranges, 15–29 Hz for global efficiency and 16–27 Hz for local efficiency, and we observed an additional increase in both graph measures around 60 Hz (γ-band) (Fig. 3C–D). These results suggest that anticipatory network effects enhance large-scale network communication especially in the β-band, by changing network topology at these frequencies to favor functional integration both globally and within functional subgraphs.

3.3. Anticipatory stage: absence of local pac changes

In the prestimulus window, we found that attention to both motion and orientation enhanced the levels of functional integration in the cortical network in the β-band. For the Attended-orientation condition, we also observed significant increases of these levels in the γ-band, compared to Unattended. The activity from the two frequency bands may be integrated locally through mechanisms of cross-frequency coupling (Bonnefond et al., 2017; Buzsáki, 2006; Canolty et al., 2006; Canolty and Knight, 2010; Jensen and Colgin, 2007), we thus investigated whether attention modulates local PAC. For this analysis, we focused on the occipito-temporal ROIs and calculated within-region PAC (Martínez-Cancino et al., 2019; Penny et al., 2008). In each participant and task condition, a surrogate analysis was used to test for the presence of local PAC (see Methods). This test did not reveal any statistically significant β-γ PAC, which indicates that network-level changes in the γ-band for Attended-orientation are unlikely to results from linear interactions between β and γ frequencies at the local level.

3.4. Anticipatory stage: brief summary

Together, the analyses in the prestimulus window revealed that anticipatory attention-induced modulations facilitate network-level communication in the β-band. This confirms our hypothesis of a central role of β-rhythmic modulations in the anticipatory stage of attention. We further expected the presence of anticipatory α-rhythmic modulations for task-irrelevant (unattended) signals, but we did not find any major role for anticipatory modulations of α activity in our data.

3.5. Reactive stage: attention dynamically modulates brain rhythms

To characterize the attentional modulations of neuronal rhythms in the reactive stage of processing, time-varying power estimates in each ROI were compared between Attended and Unattended conditions in time-frequency space (time frames in the window 0–500 ms and frequencies in the range 1–100 Hz).

The results showed reactive differences due to attention, characterized by significantly higher α and β-band power in Unattended compared to Attended conditions over several fronto-parietal and occipito-temporal ROIs. For the comparison between Attended-motion and Unattended, we found significant decreases in PM L and R (p_{perm}<0.05), SMA and MCC (p_{perm}<0.005), V1 R (p_{perm}<0.001), Cuneus (p_{perm}<0.001), GPC L (p_{perm}<0.001), SPL L and R (p_{perm}<0.001), IPL L and R (p_{perm}<0.05), and MTG L and V5 R (p_{perm}<0.05) (Fig. 4A). For the comparison between Attended-orientation and Unattended, we found significant power decreases in PM L and R (p_{perm}=0.05), MFG R (p_{perm}<0.05), SMA and MCC (p_{perm}<0.005), V1 L (p_{perm}<0.05), V1 R (p_{perm}<0.0005), Cuneus (p_{perm}<0.0005), GPC L (p_{perm}<0.005), SPL L and R (p_{perm}<0.0005), IPL L (p_{perm}<0.05), IPL R (p_{perm}<0.01), and MTG L (p_{perm}<0.05) (Fig. 4B). In this second comparison, we also found increases in FFG L (p_{perm}<0.01), at frequencies in the γ-band.

The observed power differences between task conditions could in principle be due to stimulus-evoked increases or decreases, in either of the two conditions. We therefore inspected time-varying relative power change with respect to baseline, in each task condition separately (Figs. S2–S4, Supplementary material). This showed that power differences in the α and β-band reflected an ERD (Minami et al., 2014; Pfurtscheller and Lopes da Silva, 1999; Schmiedt et al., 2014;

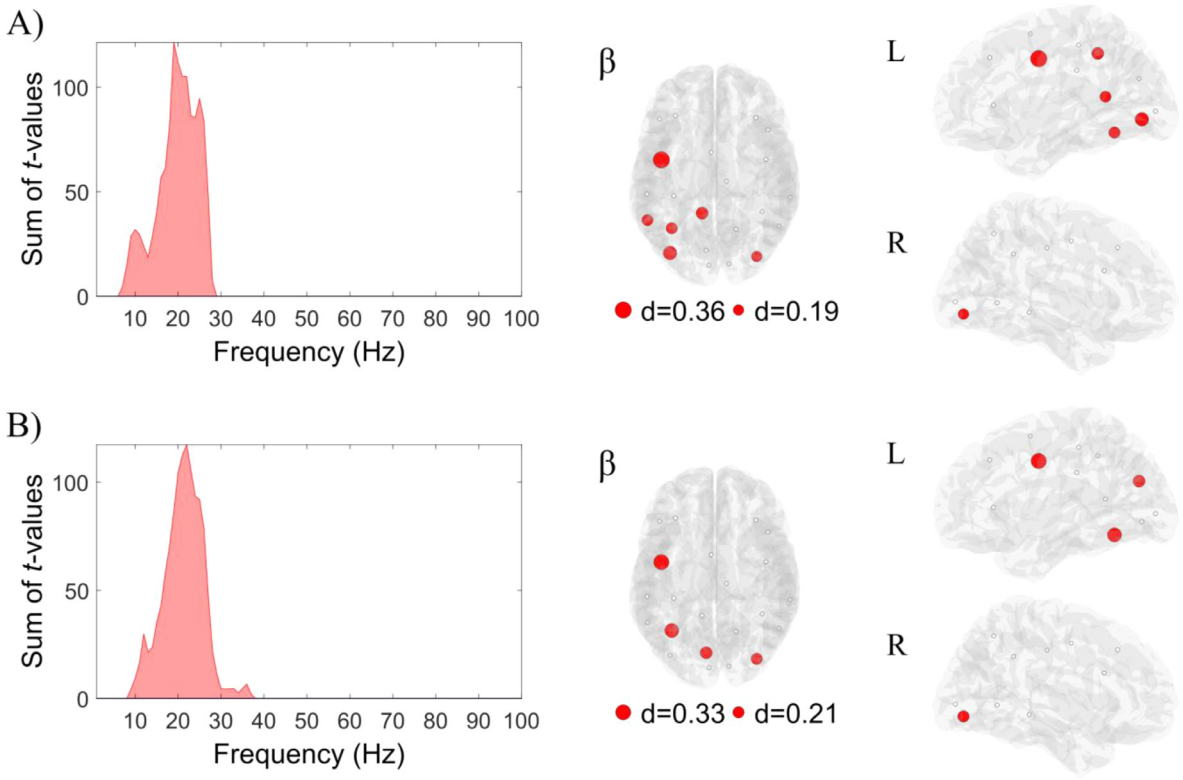

Fig. 2. Anticipatory stage: attentional modulations of neuronal rhythms. Results for the comparisons between A) Attended-motion and Unattended and B) Attended-orientation and Unattended. Each figure shows the frequency distribution of the sum of statistically significant differences across ROIs (positive *t*-values for Attended-motion higher than Unattended, and vice versa negative *t*-values), obtained from cluster-based permutation (two-tailed dependent *t*-test with $p<0.05$, 50,000 permutations, and $p<0.05$ for the permutation test). Here and in the following, red indicate positive differences between Attended and Unattended conditions (i.e., increases with attention), blue indicates negative differences (i.e., decreases with attention). In each figure, the effect sizes in the β-band (15–30 Hz) for each ROI of power differences between conditions are superimposed over the MNI template, with diameters corresponding to effect size. Effect sizes were estimated using Cohen's *d* (Cohen, 1992). Lateral views of the left (L) and right (R) hemispheres, separately, are also shown.

Yordanova et al., 2001) that was larger for attended than unattended stimuli (Mazaheri and Picton, 2005; Pascucci et al., 2018). In the Unattended condition, such α and β ERD was small or absent in frontal and parietal ROIs (Fig. S2, Supplementary material). We also observed within-region event-related synchronization (ERS) at higher frequencies (γ-band), especially for the Attended conditions. In the Attended-motion in particular, a sharp γ ERS was present in right occipito-temporal ROIs (V2 R, V5 R, and MTG R), peaking at latencies around 100 ms after stimulus onset (Fig. S3, Supplementary material). It is worth highlighting that V5–MTG are known to be specialized for the perception of motion (Ahlfors et al., 1999; Schoenfeld et al., 2007), suggesting that local reactive effects selectively involved functionally specialized regions. For Attended-orientation, γ ERS was less pronounced in occipital ROIs (e.g., V2 and FFG) (Fig. S4, Supplementary material).

Taken together, our results show that attention modulates local neuronal rhythms in distinct ways before and after stimulus onset. Anticipatory effects involved attentional increase of β-band power, while reactive effects involved stronger α and β-band ERD due to attention, especially in parietal and frontal regions.

3.6. Reactive stage: dynamic changes in local α-γ coupling

Rhythms in the α-band have been proposed to gate attention through pulsed inhibition that suppresses the functional processing and interareal γ-band communication (Jensen and Mazaheri, 2010). A reactive release from inhibitory gating (α ERD) with attention may selectively enhance the processing of task-relevant sensory signals (γ ERS), and modulations in the structures of α-γ PAC in sensory areas may mediate this mechanism (Bonnefond and Jensen, 2015; Haegens et al., 2011b; Mathewson et al., 2011; Mazaheri and Jensen, 2010; Pascucci et al., 2018; Popov et al., 2017).

To assess attention-induced α-γ PAC changes dynamically, we used a time-varying measure of α-γ coupling over time frames (0–500 ms after stimulus onset), using a fixed central frequency for the phase time series in α-band (10 Hz) and varying the central frequency for the amplitude time series in γ (see Methods). The results of a surrogate analysis revealed the presence of significant α-γ PAC estimates across participants and task conditions, primarily for time frames in the interval 100–200 ms poststimulus (Fig. S5, Supplementary material). We then compared significant (masked) estimates between Attended and Unattended conditions, and the results revealed the presence of dynamic attentional increases in α-γ PAC in several occipital and temporal ROIs (Fig. 5). For the comparison between Attended-motion and Unattended, we found significant α-γ PAC increases ($p_{perm}<0.05$) in Cuneus, V2 R, V5 R, and MTG R (Fig. 5A). For the comparison between Attended-orientation and Unattended, significant α-γ PAC increases were obtained in V1 L and V2 L ($p_{perm}<0.05$), Cuneus and V2 R (Positive: $p_{perm}<0.005$), and MTG L ($p_{perm}<0.01$) (Fig. 5B).

A control analysis based on stratification (Aru et al., 2015) confirmed that the observed effects could not be attributed to power differences in the signals between conditions (Fig. S6, Supplementary material). In sum, while certain regions showed general attentional modulations of PAC (Cuneus, V2 R), others showed effects that were specific of the attended feature: V5 R and MTG R for motion; V1 L, V2 L, and MTG-L for orientation. To directly assess the specificity of these α-γ PAC modulations depending on the attended feature, we also compared the two Attended conditions. The results showed significant α-γ PAC increases

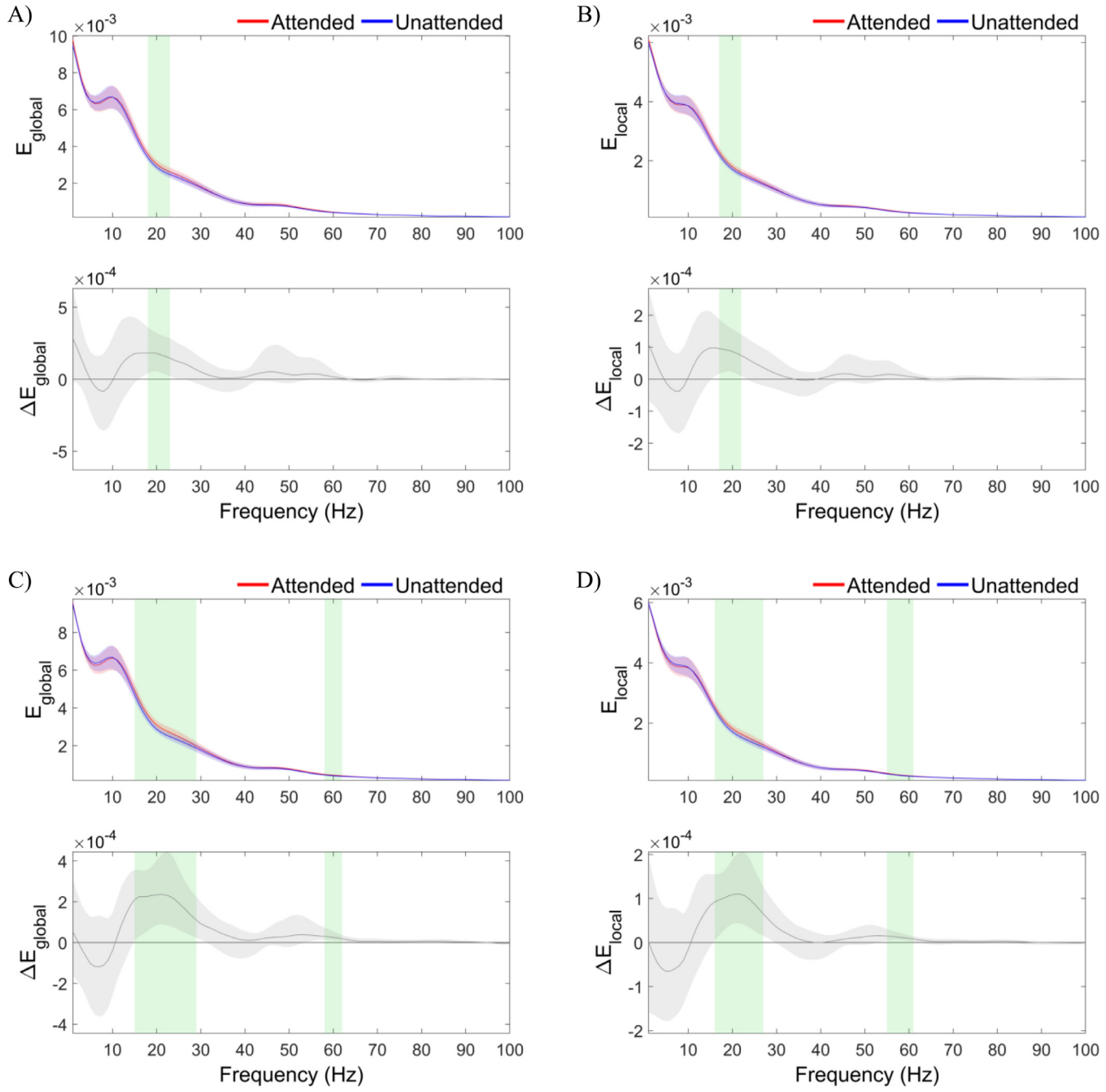

Fig. 3. Anticipatory stage: differences in network efficiency. The results for global (E_{global}) and local network efficiency (E_{local}) are shown for the comparison between Attended-motion and Unattended (A–B), and for the comparison between Attended-orientation and Unattended (C–D). Each figure shows the grand-average across participants of graph measure estimates in each condition (top, Attended in red and Unattended in blue) and the differences between conditions (ΔE_{global} and ΔE_{local}; bottom, in gray), as a function of frequency. Shadings represent the standard error of the mean, frequencies that showed statistically significant results in a two-tailed dependent *t*-test (p_{FDR}<0.05) are highlighted in green.

(p_{perm}<0.05) for Attended-motion compared to Attended-orientation in V5 R and MTG R, vice versa in V1 L (Fig. S7, Supplementary material).

Non-stationarities in neural data that are unrelated to genuine PAC, can produce correlations between frequency components that may be misinterpreted as PAC increases (Aru et al., 2015; Gardner et al., 2006). Non-stationarities are typically observed in stimulus-evoked potentials and affect a broad range of frequency components. Therefore we used methods specifically developed to measure event-related PAC with respect to stimulus onset, which should in principle avoid artifacts due to event-related non-stationarities in the signals (Martínez-Cancino et al., 2019; Pascucci et al., 2018; Voytek et al., 2013). However, these methods succeed in this purpose only for precise repeated responses, where stationarity over trials is maintained, a condition that often is not met in real neural data due to slight jitter between response times (Aru et al., 2015). We thus checked the differences in non-stationarities across trials between Attended and Unattended conditions, by computing mean and variance across trials in each task condition and comparing them between conditions. The resulting between-condition differences in non-stationarities did not allow to directly predict the reactive attentional modulations of α-γ PAC, suggesting that these may not be simply caused by such event-related artifacts (Figs. S8–S9, Supplementary material). Additionally we repeated the reactive PAC analysis on signals obtained

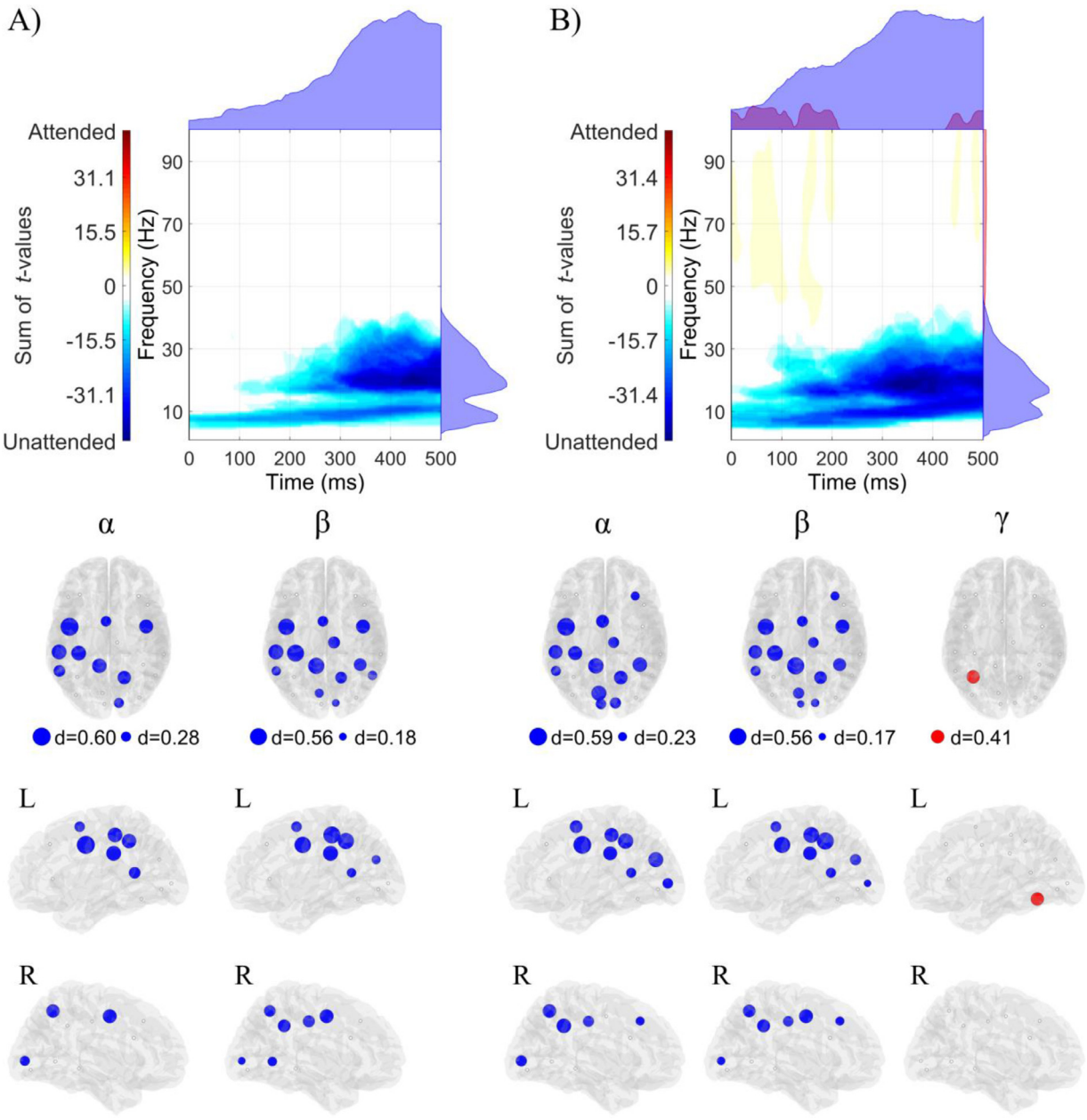

Fig. 4. Reactive stage: attentional modulations of neuronal rhythms. Results for the comparison between A) Attended-motion and Unattended and B) Attended-orientation and Unattended. Each figure shows the time-frequency distribution of the sum of statistically significant differences across ROIs, obtained from cluster-based permutation (two-tailed dependent *t*-test with $p<0.05$, 50,000 permutations, and $p<0.05$ for the permutation test). The marginal plots show time- or frequency-collapsed distributions of all significant power differences. In each figure, the effect sizes in one frequency band for each ROI of power differences between conditions are superimposed over the MNI template (first row), with diameters corresponding to effect size. Effect sizes were estimated using Cohen's *d* (Cohen, 1992). Lateral views of the left (L) and right (R) hemispheres, separately, are also shown (second and third row). Frequency bands were defined as: α (8–12 Hz), β (15–30 Hz), and γ (45–100 Hz).

after subtracting the trials mean and dividing by the trials standard deviation (normalization), point-by-point for each single-trial signal, which are two steps typically adopted to remove non-stationarity across trials in connectivity analyses (see, e.g., Ding et al., 2000). The results of this analysis confirmed the presence of significant α-γ PAC increases with attention, in V5 R and MTG R for motion and in V1 L for orientation (Fig. S10, Supplementary material).

3.7. Reactive stage: fast dynamics of network efficiency

We next asked how attentional processing affects large-scale network topology after stimulus onset. For this assessment we derived time- and frequency-resolved global efficiency and local efficiency of the network from time-varying iPDC estimates, and compared them between conditions over time frames (0–500 ms) and frequencies (1–100 Hz) (see Methods).

The results showed significantly diminished global ($p_{perm}<0.01$) and local network efficiency ($p_{perm}<0.05$) for Attended-motion compared to Unattended, in the α and β-band starting from around 270 ms after stimulus onset (Fig. 6A–B). Similar results were obtained by comparing Attended-orientation and Unattended, with significantly decreased global ($p_{perm}<0.005$) and local efficiency ($p_{perm}<0.01$) in α and β frequencies (Fig. 6C–D). Here, significant low-frequency differences emerged after 230 ms poststimulus, and were preceded by a

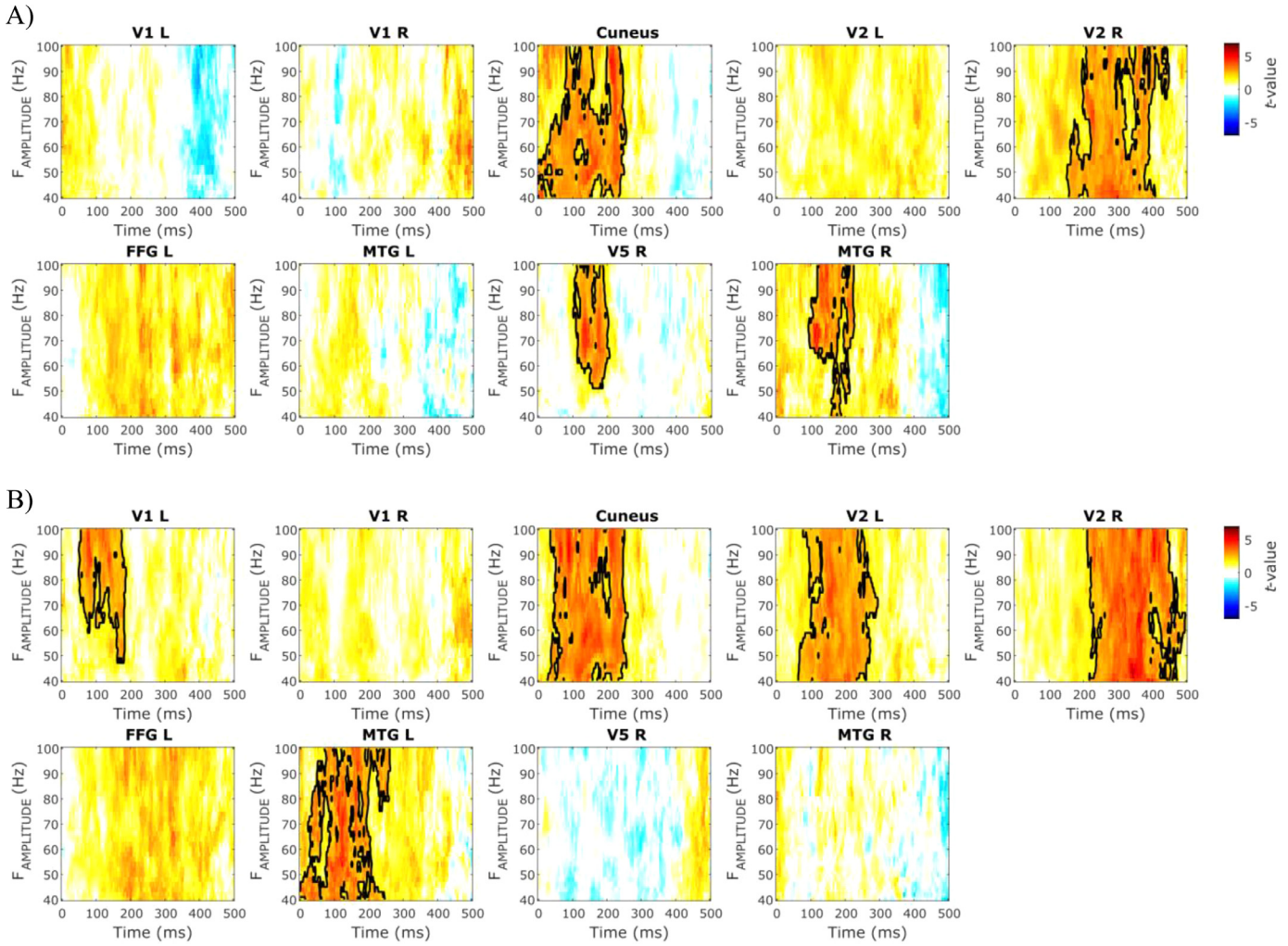

Fig. 5. Reactive stage: dynamic differences in within-region α-γ PAC. Temporal evolution of within-region PAC changes for coupling between α-band phase (10 Hz) and γ-band amplitude (40–100 Hz, in 2Hz-steps). Shown are comparisons between A) Attended-motion and Unattended and B) Attended-orientation and Unattended. Statistically significant results from cluster-based permutation approach (two-tailed dependent *t*-test with $p<0.05$, 50,000 permutations, and $p<0.05$ for the permutation test) are highlighted by the black outlines.

significant γ-band increase of both graph measures for Attended-orientation (above 40 Hz and at latencies between 170 and 220 ms poststimulus; $p_{perm}<0.05$). A trend for attention-induced γ increases was present for Attended-motion in the 100–300 ms time window, but did not reach statistical significance (Fig. S11, Supplementary material, shows unthresholded results).

3.8. Reactive stage: brief summary

In the reactive stage of attentional processing, our analyses provided two main findings: i) α-band desynchronization patterns in areas of the fronto-parietal network are accompanied by increased γ-band synchronization in occipito-temporal cortices, where specific α-driven structures of nested oscillations (α-γ) emerged dynamically, depending on the attended feature; ii) attention-related whole-brain connectivity changes first facilitate network-level communication in the γ-band, and then impede it in the α and β-band. These findings confirm our hypotheses of α-γ coupling increases due to attention in visual cortices (i), and of the presence of inverse between-frequencies relationship for network-level interactions mediating the processing of task-relevant signals (ii).

4. Discussion

In the present work, we sought to characterize local and large-scale neuronal dynamics during anticipatory and reactive stages of feature-based selective attention. To this aim, we investigated local cross-frequency coupling and brain-wide directed connectivity during a visual discrimination task that required the attentional selection of one of two spatially overlapping features. Our results show distinct patterns of nested oscillations and functional network topologies that precede and follow stimulus onset. More precisely, we found evidence for a dominant role of β rhythms in the anticipatory stage, followed by stimulus-evoked α-band desynchronization patterns and α-driven structures of nested oscillations. The use of a control condition and the presentation of overlapping features at a single location also allowed us to disentangle between general effects of stimulus relevance and specific effects of the attended feature (motion or orientation). Fig. 7 summarizes our findings.

Feature-based selective attention was mediated by a stimulus-induced reconfiguration of both local and large-scale neuronal interactions. Before stimulus onset, local β power increases in left prefrontal cortex and occipito-temporal regions were paralleled by increased levels of network integration in the β-band. After stimulus onset, brain activity underwent a marked reconfiguration, with robust desynchronization of α rhythms and increased α-γ coupling in feature-selective regions

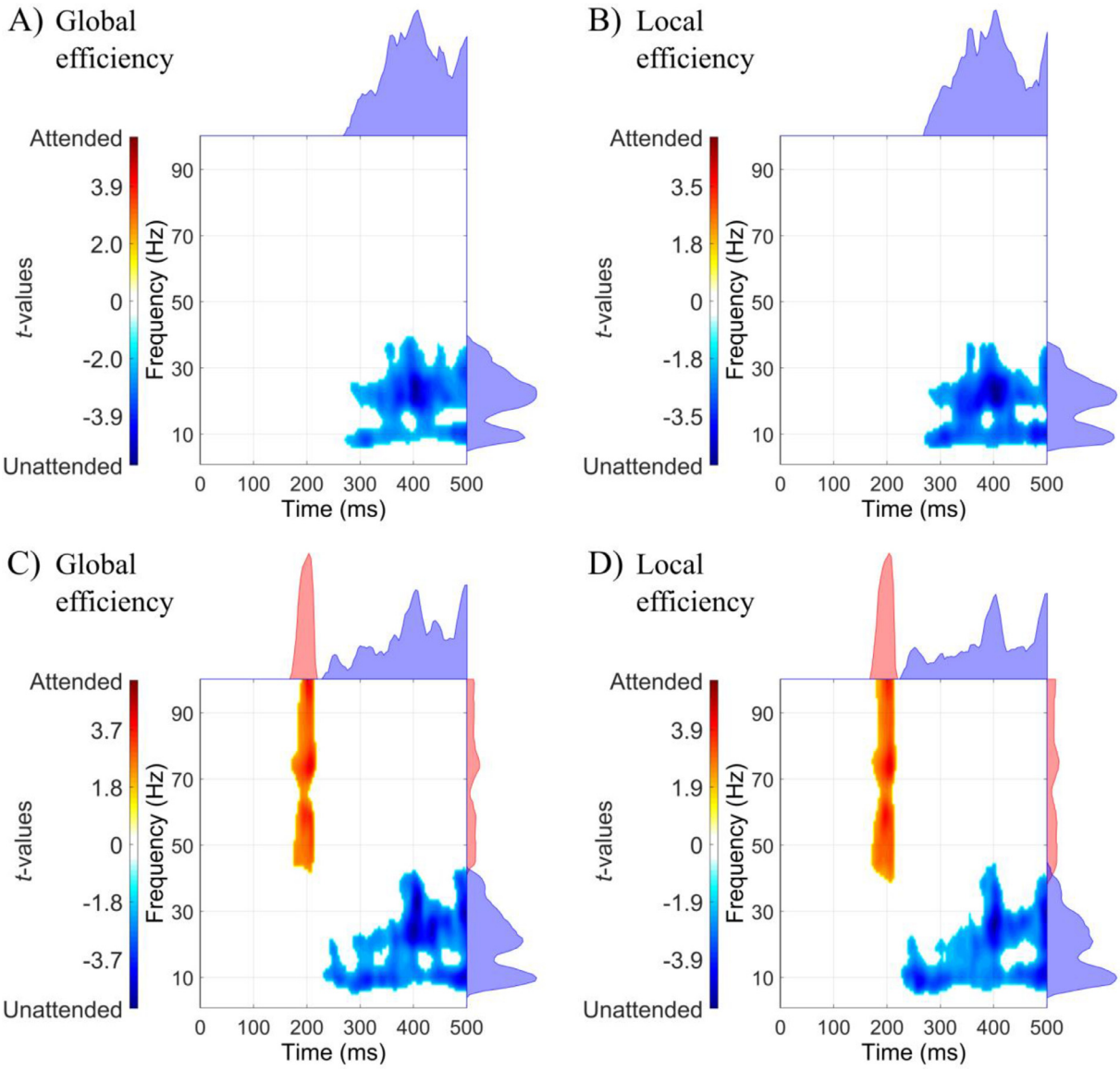

Fig. 6. Reactive stage: dynamic differences in network efficiency. The results for global (left) and local network efficiency (right) are shown for the comparison between Attended-motion and Unattended (A–B), and for the comparison between Attended-orientation and Unattended (C–D). Each figure shows the time-frequency distribution of significant differences, obtained from cluster-based permutation (two-tailed dependent *t*-test with $p<0.05$, 50,000 permutations, and $p<0.05$ for the permutation test). The marginal plots show time- and frequency-collapsed distributions of significant differences.

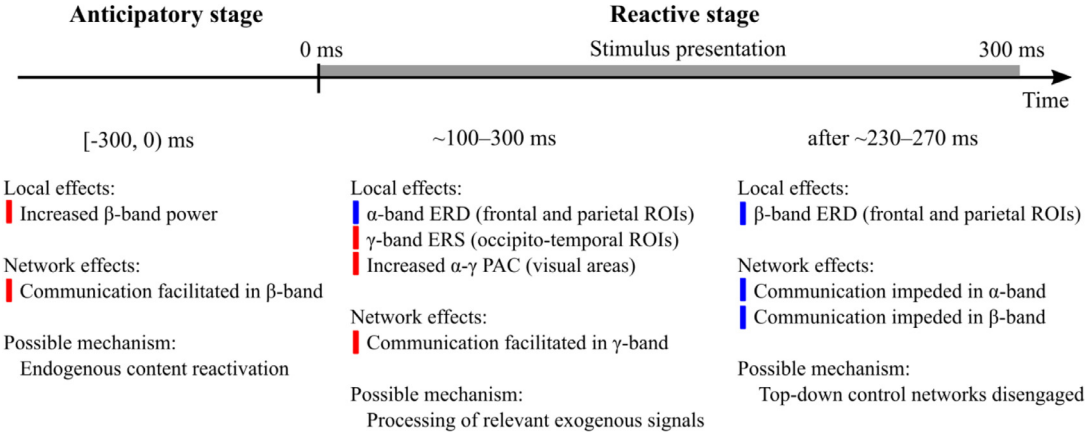

Fig. 7. Temporal sequence of attention-induced effects. The figure highlights the sequential evolution of local and network-level effects observed in the present study, from the anticipatory to the reactive stage of selective attention (from left to right), with respect to stimulus onset (*0 ms*). Red/blue patches indicate attention-induced increases/decreases.

(V5 and MTG in the right hemisphere for motion discrimination; V1 for orientation discrimination), as well as in other visual areas (Cuneus and right V2). The observed cascade of attention-related effects suggests that different mechanisms, involving the interplay between large-scale dynamics and nested oscillations, serve distinct aspects of selective attention.

Prestimulus β-band activity may reflect an increase in functional communication among regions involved in the upcoming task. Interpreting the role of β rhythms in the context of attention and cognitive processing, however, is not trivial, given the large body of work traditionally relating these rhythms to motor control (Pfurtscheller et al., 1996; Pogosyan et al., 2009; Sanes and Donoghue, 1993; Swann et al., 2009), sensorimotor functions (Lalo et al., 2007) and working memory (Lundqvist et al., 2016; Schneider and Rose, 2016; Siegel et al., 2009). A recent line of evidence has associated β rhythms with the maintenance of the status quo, that is, the preservation of ongoing sensorimotor states and cognitive sets (Engel and Fries, 2010). Following this line, other studies have hypothesized a role for β-band synchronization in establishing flexible networks of neuronal ensembles that carry content- and task-specific representations (Antzoulatos and Miller, 2016, 2014; Buschman et al., 2012; Spitzer and Haegens, 2017). Our results appear in agreement with this latter definition, by showing that large-scale network interactions associated with β rhythms may control endogenous mechanisms of attention before stimulus onset, likely conveying task-related information to downstream areas (e.g., the relevant stimulus feature, the type of response required) (Richter et al., 2017).

It is relevant to note that, contrary to previous reports (see Chelazzi et al., 2019; Foster and Awh, 2019; Snyder and Foxe, 2010 for reviews and discussions), we found no major role for anticipatory modulations of α-band activity in our data. While, at first, this seems to support the alternative view of α rhythms as a secondary type of inhibitory mechanism, observable only in relation to target processing (e.g., at ipsilateral sides of relevant stimuli; Chelazzi et al., 2019; Foster and Awh, 2019), the fact that our analysis always involved subtracting a control condition with identical stimulation could have hindered anticipatory increases in α power reflecting aspecific preparatory stages and dynamic reallocations of attentional resources (van Diepen and Mazaheri, 2017).

A clear modulation of α-band activity was evident shortly after stimulus onset. Alpha desynchronization (Mazaheri and Picton, 2005; Pfurtscheller and Lopes da Silva, 1999) was the main component determining the observed network reconfiguration, accompanied by local increases of α-γ coupling in task-relevant sensory regions. This latter phenomenon is in line with recent accounts hypothesizing a role of α rhythms in aligning the phase of high-frequency oscillations carrying relevant processing (Bonnefond et al., 2017; Pascucci et al., 2018). Under this view, the decrease of α power resulting from the evoked desynchronization would allow longer windows of neuronal excitability, favoring local increases and feedforward propagation of γ-band activity (Bonnefond et al., 2017). Thus, the co-occurrence of α desynchronization and α-γ coupling may underlie the emergence of short functional windows where the release from inhibitory signals enhances sensory and task-relevant processing. In this respect, our results are also in agreement with the gating-by-inhibition hypothesis that postulates a similar inverse relationship between the degree of α-band synchronization and the level of local neuronal excitability and γ-band activity (Bonnefond and Jensen, 2015; Haegens et al., 2011b; Jensen and Mazaheri, 2010; Mathewson et al., 2011; Mazaheri and Jensen, 2010).

Adding to the gating-by-inhibition framework (Mazaheri and Jensen, 2010), we found that the effects of release from inhibitory gating specifically involved cortical regions encoding the attended feature: motion coherence in right V5–MTG (Ahlfors et al., 1999; Schoenfeld et al., 2007), and Gabor's orientation in primary visual cortex (V1) (Bosking et al., 1997; Dupont et al., 1998; Koelewijn et al., 2011; Simoncelli and Olshausen, 2001), in addition to less task-specific areas. A compelling question for future investigations is whether these reactive α-driven mechanisms of local cross-frequency coupling underlie also the attentional selection based on whole-object representations, for example of faces and houses via the selective involvement of fusiform face area and parahippocampal place area, respectively. Furthermore, stimulation techniques could help to establish whether sensory areas that showed attentional PAC modulations are causally relevant for behavior, and potentially help increase their functioning (see, e.g., Riddle et al., 2019). In particular α-rhythmic transcranial magnetic stimulation (TMS) over feature-selective ROIs (e.g., V5–MTG for motion), delivered before stimulus onset, should reduce the receptivity of these areas to top-down oscillatory signals that control sensory gating (Fiebelkorn and Kastner, 2019; Jensen and Mazaheri, 2010). This way, TMS could help increase selective attention and positively impact behavioral performance in specific task conditions (e.g., when motion is attended). Alternatively, the specific timing of stimulations may reset the ongoing phases of local neuronal oscillations in such a way that α-band inter-areal coherence and large-scale communication increase, producing opposite effects on attention. Analogous assessments could be carried out by using γ TMS stimulations.

In analyzing cross-frequency coupling and its changes across experimental conditions, a certain number of possible issues and confounds should be taken into consideration. We adopted control analyses based on surrogate testing and a stratification procedure, respectively, for assessing the statistical significance of PAC estimates and dealing with confounds due to differences in power between conditions (Aru et al., 2015; Martínez-Cancino et al., 2019). Another source of confounds for PAC analysis comes from unspecific non-stationarities, i.e., those that are not related to or caused by genuine coupling of neural processes, and may result in spurious PAC estimates (Aru et al., 2015). To address confounds driven by non-stationarities, for each ROI and task condition we quantified non-stationarities in terms of mean and variance across trials, and compared them between Attended and Unattended conditions. In ROIs where we found attention-induced α-γ PAC increases, the presence of between-condition differences in non-stationarities would indicate that these artifactually drive PAC changes. Our results, however, showed that this was not the case. We also performed ensemble mean subtraction and normalization of signals to remove non-stationarities across trials, and then repeated the reactive PAC analysis, which confirmed the presence of attention-induced α-γ PAC changes in feature-selective regions. These additional analyses strongly suggest that the reactive PAC modulations come from genuine coupling mechanisms that depend on the feature-based attention conditions, but with the currently available methods we cannot completely exclude the possibility that residual unspecific non-stationarities drive the within-region PAC effects to some extent. Ultimately solving the issue of non-stationarities confounds requires the development of ad hoc methods for the detection of causality, which go beyond the limits of traditional Granger formalism to discern the directionality of cross-frequency effects, or the implementation of generative models that incorporate biophysical descriptions of cross-frequency interactions and model comparison approaches. Alternatively, as laid out above, approaches using additional external perturbations (e.g., TMS stimulations) might provide an ideal solution to constrain the number of possible scenarios for the observation of spurious PAC estimates (see Aru et al., 2015 for further discussion).

As a means to describe functional network properties, we used graph efficiency measures that indicate how easily signals can travel between network nodes, i.e., the degree of local and global integration, depending on the configuration of directed functional connections (Latora and Marchiori, 2001; Rubinov and Sporns, 2010). We found a rapid desynchronization of local α rhythms together with increased α-γ coupling in visual areas (~100–200 ms poststimulus), which co-occurred with the rise of large-scale γ-band interactions, with enhanced network efficiency in the γ range (170–220 ms poststimulus for orientation discrimination; a similar trend for motion discrimination ~100–300 ms poststimulus). The local activity modulations and the increased efficiency of inter-areal high-frequency communication occurred at latencies that are

consistent with high-level stimulus processing and attentional modulation (Hillyard et al., 1998; Hillyard and Anllo-Vento, 1998). This suggest a close relation between locally enhanced sensory processing of relevant exogenous signals of attended stimuli (Bonnefond and Jensen, 2015; Jensen and Mazaheri, 2010), and global network mechanisms by which attentional selection renders task-relevant stimulus content accessible to widespread circuits for later processing (e.g., decisional), through γ-frequency channel of communication (Bastos et al., 2015; Fries, 2015).

Our results also suggest distinct mechanisms for general and task-specific attentional effects. Task-specific modulations involved more local phenomena, characterized by increased coupling between α and γ-band activity during poststimulus time, and these effects were selective for functionally specialized regions. Based on the well-known specialization of these regions in processing the two types of stimulus' features used (Ahlfors et al., 1999; Bosking et al., 1997; Dupont et al., 1998; Koelewijn et al., 2011; Schoenfeld et al., 2007; Simoncelli and Olshausen, 2001), these results support the view of PAC and nested oscillations as regulatory mechanisms for the local analysis and feedforward communication of relevant sensory signals (e.g., target stimuli) (Bonnefond and Jensen, 2015; Jensen and Mazaheri, 2010; Pascucci et al., 2018). Theories of communication based on nested oscillations propose in fact that low-frequency carriers in the theta (θ, 3–7 Hz), α or β-band establish inter-areal communication at larger scales, by mediating local excitability (reflected by γ-band activity) (Bonnefond et al., 2017). Cross-frequency coupling at the local level, therefore, would coordinate γ-band activity and information routing at different scales (Buzsáki, 2006; Buzsáki and Wang, 2012; Canolty et al., 2006; Canolty and Knight, 2010; Jensen and Colgin, 2007; Penny et al., 2008; Voytek et al., 2010).

General attentional effects were mediated by prestimulus changes in spectral power and by topological changes in the brain-wide network of functional interactions. These included increased spectral power over left prefrontal cortex and occipito-temporal areas and increased network efficiency in the β-band. The results therefore point to an aspecific enhancement of large-scale network communication that facilitates information routing while preparing for an attended stimulus to appear (Buschman and Kastner, 2015; Fries, 2015). After stimulus onset, we found that attention induced desynchronization first in α and then in β-band (Klimesch et al., 2007, 2001; Mazaheri and Picton, 2005; Pascucci et al., 2018; Schmiedt et al., 2014). These stimulus-evoked effects co-occurred with a rapid sequence of frequency-specific changes in network topology, starting with enhanced network efficiency in the γ-band (~100–300 ms poststimulus), followed by reduced efficiency in the α and β-band (after ~230–270 ms poststimulus). As discussed, the earlier γ-band effects may reflect enhanced communication conveying task-relevant signals between cortical regions. The later low-frequency effects, on the other hand, indicate that stimulus-evoked α and β-band desynchronization co-occurs with network-level changes that diminish the levels of functional integration, both globally and within subgraphs (networks less integrated and segregated), thus reducing the communication through these frequency channels. These effects support the existence of two distinct top-down networks for the control of sensory gating (α-frequency channel) (Fiebelkorn and Kastner, 2019; Jensen and Mazaheri, 2010) and endogenous information routing (β-frequency channel) (Spitzer and Haegens, 2017).

Such top-down network effects may be controlled by specific areas. For connectivity analysis, we employed multivariate directed methods (Baccalá and Sameshima, 2014), and a recently developed adaptive filter that was designed for highly dynamic, non-stationary signals (Pascucci et al., 2020). While we considered a network of brain-wide cortical regions to investigate attention-induced changes in large-scale neuronal communication through distinct frequency channels, locally we focused on the phenomenon of nested oscillations for selective processing in sensory cortices. Nonetheless, frontal and parietal areas may also play a role in top-down control during selective attention. A top-down model of fronto-parietal control of attentional selection has in fact emerged from previous studies, suggesting top-down signaling from prefrontal cortex in the β-band when attention is endogenously controlled, and top-down α-band signals originating from posterior parietal cortex to disrupt sensory processing of irrelevant information (Buschman and Kastner, 2015; Buschman and Miller, 2007; Fiebelkorn and Kastner, 2020; Pascucci et al., 2018). These top-down signals could affect the local coupling in sensory areas (see, e.g., Pascucci et al., 2018). Future work is needed to address the relationships between local cross-frequency coupling and changes in incoming or outgoing connection strengths or changes in network topology, by deriving single-trial estimates of connectivity instead of using the multi-trial connectivity approach adopted here, across feature-based attention conditions.

Beyond the cortico-centric view of top-down control of attention, recent studies in non-human primates revealed that also subcortical structures like the pulvinar and mediodorsal thalamus play an important role in attentional control (Fiebelkorn et al., 2019; Saalmann et al., 2012). In this respect, despite we considered a whole-brain cortical network for our analyses, one potential limitation is linked to the presence of unobserved common inputs in subcortical structures (Bastos and Schoffelen, 2016; Pagnotta et al., 2018b). We did not include the thalamus as a ROI, due to the EEG intrinsic limitations in accurately reconstructing subcortical activity (although see Seeber et al., 2019). Hence, our results provide solely an account for the cortico-cortical interactions in mediating selective attention. In the future, the use of invasive recordings in clinical populations and implanted patients might provide further insights about the role of subcortical structures and thalamo-cortical interactions in controlling attention and other cognitive functions.

Another known methodological limitation of EEG studies is associated with the problem of spatial leakage. We employed a source reconstruction procedure using participant-specific models of electrodes and realistic head models derived from individual-participant's anatomical MRI. Source-reconstructed signals were extracted from fMRI-derived ROIs using an SVD-based approach (Rubega et al., 2019). This projection method provides reliable dimensionality reduction and helps derive an overall *"population signal"* for each brain region, by estimating signals that explain most of the variability across the entire group of dipoles in each ROI. A method based on orthogonalization was then used to correct spatial leakage between ROIs (Pascual-Marqui et al., 2017). We should caution that, however, the possible presence of residual leakage may prevent a complete separation of source-reconstructed ROIs' signals, and therefore of the local effects observed for example in right V5 and MTG (when motion was attended), or in early visual cortices (Cuneus, V1, V2).

In conclusion, we have shown that selective attention is mediated by a dynamic reorganization of frequency-specific inter-areal interactions and local activity changes. In anticipation of relevant stimuli, cortical interactions support information routing through β-frequency channels to control endogenous content reactivation. In the reactive stage of selective attention, α-driven desynchronization patterns and structures of nested oscillations in task-specific sensory areas emerge together with increased network-level communication through γ-frequency, presumably enhancing sensory processing of relevant exogenous information and rendering it more widely accessible across cortical regions for later processing. While we have here used an experimental paradigm with controlled environment and well-defined stimuli characteristics, the same approaches and analysis strategies could be employed to study selective attention in more naturalistic paradigms using naturalistic stimuli (see, e.g., Ki et al., 2016), or even recording the participants during everyday situations, like the students in a classroom setting (see, e.g., Ko et al., 2017; Poulsen et al., 2017). Moreover, the ability to flexibly adapt both whole-brain communication and selective mechanisms of local processing may play a role beyond visual attention and may underlie other cognitive functions, as well as attentional disorders such as ADHD (Bush, 2010). Likewise the approaches used here to study visual selective attention could help shed light on how they malfunc-

tion in psychiatric conditions. Alterations of the observed patterns of frequency-specific network-level communication and/or local coupling mechanisms may in fact account for certain cognitive deficits resulting from autism spectrum disorders (Sperdin et al., 2018), epilepsy (Coito et al., 2015), or schizophrenia (Friston et al., 2016).

CRediT author statement

Mattia F. Pagnotta: Conceptualization, Methodology, Software, Formal analysis, Investigation, Data Curation, Writing - original draft, Writing - review & editing, Visualization.

David Pascucci: Conceptualization, Software, Writing - original draft, Writing - review & editing.

Gijs Plomp: Conceptualization, Methodology, Writing - original draft, Writing - review & editing, Supervision, Project administration, Funding acquisition.

Declaration of Competing Interest

The authors declare that the study has been conducted in the absence of any conflict of interest.

Acknowledgements

This study was supported by the Swiss National Science Foundation (grants PP00P1_157420 and PP00P1_183714; G.P.).

Supplementary materials

Supplementary material associated with this article can be found, in the online version, at doi:10.1016/j.neuroimage.2020.117354.

References

Ahlfors, S.P., Simpson, G.V., Dale, A.M., Belliveau, J.W., Liu, A.K., Korvenoja, A., Virtanen, J., Huotilainen, M., Tootell, R.B.H., Aronen, H.J., Ilmoniemi, R.J., 1999. Spatiotemporal Activity of a Cortical Network for Processing Visual Motion Revealed by MEG and fMRI. J. Neurophysiol. 82, 2545–2555. doi:10.1152/jn.1999.82.5.2545.

Antzoulatos, E.G., Miller, E.K., 2016. Synchronous beta rhythms of frontoparietal networks support only behaviorally relevant representations. Elife 5, e17822. doi:10.7554/eLife.17822.

Antzoulatos, E.G., Miller, E.K., 2014. Increases in Functional Connectivity between Prefrontal Cortex and Striatum during Category Learning. Neuron 83, 216–225. doi:10.1016/j.neuron.2014.05.005.

Anzolin, A., Presti, P., Van De Steen, F., Astolfi, L., Haufe, S., Marinazzo, D., 2019. Quantifying the Effect of Demixing Approaches on Directed Connectivity Estimated Between Reconstructed EEG Sources. Brain Topogr 32, 655–674. doi:10.1007/s10548-019-00705-z.

Arnold, M., Milner, X.H.R., Witte, H., Bauer, R., Braun, C., 1998. Adaptive AR modeling of nonstationary time series by means of Kalman filtering. IEEE Trans. Biomed. Eng. 45, 553–562. doi:10.1109/10.668741.

Aru, Juhan, Aru, Jaan, Priesemann, V., Wibral, M., Lana, L., Pipa, G., Singer, W., Vicente, R., 2015. Untangling cross-frequency coupling in neuroscience. Curr. Opin. Neurobiol. 31, 51–61. doi:10.1016/j.conb.2014.08.002.

Astolfi, L., Cincotti, F., Mattia, D., De Vico Fallani, F., Tocci, A., Colosimo, A., Salinari, S., Marciani, M.G., Hesse, W., Witte, H., others, 2008. Tracking the time-varying cortical connectivity patterns by adaptive multivariate estimators. IEEE Trans. Biomed. Eng. 55, 902–913. doi:10.1109/TBME.2007.905419.

Baccalá, L.A., Sameshima, K., 2014. Partial Directed Coherence. In: Methods in Brain Connectivity Inference through Multivariate Time Series Analysis, Frontiers in Neuroengineering Series. CRC Press, pp. 57–73. doi:10.1201/b16550-6.

Bach, M., 1996. The Freiburg Visual Acuity Test–Automatic Measurement of Visual Acuity. Optom. Vis. Sci. 73, 49–53. doi:10.1097/00006324-199601000-00008.

Baldauf, D., Desimone, R., 2014. Neural Mechanisms of Object-Based Attention. Science 344, 424–427. doi:10.1126/science.1247003.

Bastos, A.M., Schoffelen, J.-.M., 2016. A Tutorial Review of Functional Connectivity Analysis Methods and Their Interpretational Pitfalls. Front. Syst. Neurosci. 9. doi:10.3389/fnsys.2015.00175.

Bastos, A.M., Vezoli, J., Bosman, C.A., Schoffelen, J.-.M., Oostenveld, R., Dowdall, J.R., De Weerd, P., Kennedy, H., Fries, P., 2015. Visual Areas Exert Feedforward and Feedback Influences through Distinct Frequency Channels. Neuron 85, 390–401. doi:10.1016/j.neuron.2014.12.018.

Bigdely-Shamlo, N., Mullen, T., Kothe, C., Su, K.-.M., Robbins, K.A., 2015. The PREP pipeline: standardized preprocessing for large-scale EEG analysis. Front. Neuroinformatics 9. doi:10.3389/fninf.2015.00016.

Bonnefond, M., Jensen, O., 2015. Gamma Activity Coupled to Alpha Phase as a Mechanism for Top-Down Controlled Gating. PLoS ONE 10, e0128667. doi:10.1371/journal.pone.0128667.

Bonnefond, M., Kastner, S., Jensen, O., 2017. Communication between Brain Areas Based on Nested Oscillations. eNeuro 4. doi:10.1523/ENEURO.0153-16.2017, ENEURO.0153-16.2017.

Bosking, W.H., Zhang, Y., Schofield, B., Fitzpatrick, D., 1997. Orientation Selectivity and the Arrangement of Horizontal Connections in Tree Shrew Striate Cortex. J. Neurosci. 17, 2112–2127. doi:10.1523/JNEUROSCI.17-06-02112.1997.

Brunner, C., Billinger, M., Seeber, M., Mullen, T.R., Makeig, S., 2016. Volume Conduction Influences Scalp-Based Connectivity Estimates. Front. Comput. Neurosci. 10. doi:10.3389/fncom.2016.00121.

Buschman, T.J., Denovellis, E.L., Diogo, C., Bullock, D., Miller, E.K., 2012. Synchronous Oscillatory Neural Ensembles for Rules in the Prefrontal Cortex. Neuron 76, 838–846. doi:10.1016/j.neuron.2012.09.029.

Buschman, T.J., Kastner, S., 2015. From Behavior to Neural Dynamics: An Integrated Theory of Attention. Neuron 88, 127–144. doi:10.1016/j.neuron.2015.09.017.

Buschman, T.J., Miller, E.K., 2007. Top-Down Versus Bottom-Up Control of Attention in the Prefrontal and Posterior Parietal Cortices. Science 315, 1860–1862. doi:10.1126/science.1138071.

Bush, G., 2010. Attention-Deficit/Hyperactivity Disorder and Attention Networks. Neuropsychopharmacology 35, 278–300. doi:10.1038/npp.2009.120.

Buzsáki, G., 2006. Rhythms of the Brain. Oxford University Press doi:10.1093/acprof:oso/9780195301069.001.0001.

Buzsáki, G., Draguhn, A., 2004. Neuronal Oscillations in Cortical Networks. Science 304, 1926–1929. doi:10.1126/science.1099745.

Buzsáki, G., Wang, X.-.J., 2012. Mechanisms of Gamma Oscillations. Annu. Rev. Neurosci. 35, 203–225. doi:10.1146/annurev-neuro-062111-150444.

Canolty, R.T., Edwards, E., Dalal, S.S., Soltani, M., Nagarajan, S.S., Kirsch, H.E., Berger, M.S., Barbaro, N.M., Knight, R.T., 2006. High Gamma Power Is Phase-Locked to Theta Oscillations in Human Neocortex. Science 313, 1626–1628. doi:10.1126/science.1128115.

Canolty, R.T., Knight, R.T., 2010. The functional role of cross-frequency coupling. Trends Cogn. Sci. 14, 506–515. doi:10.1016/j.tics.2010.09.001.

Canolty, R.T., Soltani, M., Dalal, S.S., Edwards, E., Dronkers, N.F., Nagarajan, S.S., Kirsch, H.E., Barbaro, N.M., Knight, R.T., 2007. Spatiotemporal dynamics of word processing in the human brain. Front. Neurosci. 1, 185–196. doi:10.3389/neuro.01.1.1.014.2007.

Carrasco, M., 2011. Visual attention: The past 25 years. Vision Res 51, 1484–1525. doi:10.1016/j.visres.2011.04.012.

Chelazzi, L., Marini, F., Pascucci, D., Turatto, M., 2019. Getting rid of visual distractors: the why, when, how, and where. Curr. Opin. Psychol. 29, 135–147. doi:10.1016/j.copsyc.2019.02.004.

Cohen, J., 1992. A power primer. Psychol. Bull. 112, 155–159. doi:10.1037/0033-2909.112.1.155.

Coito, A., Plomp, G., Genetti, M., Abela, E., Wiest, R., Seeck, M., Michel, C.M., Vulliemoz, S., 2015. Dynamic directed interictal connectivity in left and right temporal lobe epilepsy. Epilepsia 56, 207–217. doi:10.1111/epi.12904.

Corbetta, M., Shulman, G.L., 2002. Control of goal-directed and stimulus-driven attention in the brain. Nat. Rev. Neurosci. 3, 201–215. doi:10.1038/nrn755.

Delorme, A., Makeig, S., 2004. EEGLAB: an open source toolbox for analysis of single-trial EEG dynamics including independent component analysis. J. Neurosci. Methods 134, 9–21. doi:10.1016/j.jneumeth.2003.10.009.

Delorme, A., Mullen, T., Kothe, C., Akalin Acar, Z., Bigdely-Shamlo, N., Vankov, A., Makeig, S., 2011. EEGLAB, SIFT, NFT, BCILAB, and ERICA: New Tools for Advanced EEG Processing. Comput. Intell. Neurosci. 2011, 1–12. doi:10.1155/2011/130714.

Ding, M., Bressler, S.L., Yang, W., Liang, H., 2000. Short-window spectral analysis of cortical event-related potentials by adaptive multivariate autoregressive modeling: data preprocessing, model validation, and variability assessment. Biol. Cybern. 83, 35–45. doi:10.1007/s004229900137.

Dupont, P., Vogels, R., Vandenberghe, R., Rosier, A., Cornette, L., Bormans, G., Mortelmans, L., Orban, G.A., 1998. Regions in the human brain activated by simultaneous orientation discrimination: a study with positron emission tomography. Eur. J. Neurosci. 10, 3689–3699. doi:10.1046/j.1460-9568.1998.00376.x.

Engel, A.K., Fries, P., 2010. Beta-band oscillations—Signalling the status quo? Curr. Opin. Neurobiol 20, 156–165. doi:10.1016/j.conb.2010.02.015.

Fiebelkorn, I.C., Kastner, S., 2020. Functional Specialization in the Attention Network. Annu. Rev. Psychol. 71. doi:10.1146/annurev-psych-010418-103429, annurev-psych-010418-103429.

Fiebelkorn, I.C., Kastner, S., 2019. A Rhythmic Theory of Attention. Trends Cogn. Sci. 23, 87–101. doi:10.1016/j.tics.2018.11.009.

Fiebelkorn, I.C., Pinsk, M.A., Kastner, S., 2019. The mediodorsal pulvinar coordinates the macaque fronto-parietal network during rhythmic spatial attention. Nat. Commun. 10, 215. doi:10.1038/s41467-018-08151-4.

Foster, J.J., Awh, E., 2019. The role of alpha oscillations in spatial attention: limited evidence for a suppression account. Curr. Opin. Psychol. 29, 34–40. doi:10.1016/j.copsyc.2018.11.001.

Foxe, J.J., Snyder, A.C., 2011. The Role of Alpha-Band Brain Oscillations as a Sensory Suppression Mechanism during Selective Attention. Front. Psychol. 2. doi:10.3389/fpsyg.2011.00154.

Fries, P., 2015. Rhythms for Cognition: Communication through Coherence. Neuron 88, 220–235. doi:10.1016/j.neuron.2015.09.034.

Friston, K., Brown, H.R., Siemerkus, J., Stephan, K.E., 2016. The dysconnection hypothesis (2016). Schizophr. Res. 176, 83–94. doi:10.1016/j.schres.2016.07.014.

Gardner, W.A., Napolitano, A., Paura, L., 2006. Cyclostationarity: Half a century of research. Signal Process 86, 639–697. doi:10.1016/j.sigpro.2005.06.016.

Geweke, J.F., 1984. Measures of conditional linear dependence and feedback between time series. J. Am. Stat. Assoc. 79, 907–915. doi:10.2307/2288723.
Granger, C.W.J., 1969. Investigating Causal Relations by Econometric Models and Cross-spectral Methods. Econometrica 37, 424–438. doi:10.2307/1912791.
Greenberg, A.S., Esterman, M., Wilson, D., Serences, J.T., Yantis, S., 2010. Control of Spatial and Feature-Based Attention in Frontoparietal Cortex. J. Neurosci. 30, 14330–14339. doi:10.1523/JNEUROSCI.4248-09.2010.
Haegens, S., Handel, B.F., Jensen, O., 2011a. Top-Down Controlled Alpha Band Activity in Somatosensory Areas Determines Behavioral Performance in a Discrimination Task. J. Neurosci. 31, 5197–5204. doi:10.1523/JNEUROSCI.5199-10.2011.
Haegens, S., Nácher, V., Luna, R., Romo, R., Jensen, O., 2011b. α-Oscillations in the monkey sensorimotor network influence discrimination performance by rhythmical inhibition of neuronal spiking. Proc. Natl. Acad. Sci. 108, 19377–19382. doi:10.1073/pnas.1117190108.
Hamalainen, M.S., Sarvas, J., 1989. Realistic conductivity geometry model of the human head for interpretation of neuromagnetic data. IEEE Trans. Biomed. Eng. 36, 165–171. doi:10.1109/10.16463.
Hansen, P.C., 1987. The truncatedSVD as a method for regularization. BIT 27, 534–553. doi:10.1007/BF01937276.
Hillyard, S.A., Anllo-Vento, L., 1998. Event-related brain potentials in the study of visual selective attention. Proc. Natl. Acad. Sci. 95, 781–787. doi:10.1073/pnas.95.3.781.
Hillyard, S.A., Vogel, E.K., Luck, S.J., 1998. Sensory gain control (amplification) as a mechanism of selective attention: electrophysiological and neuroimaging evidence. Philos. Trans. R. Soc. Lond. B. Biol. Sci. 353, 1257–1270. doi:10.1098/rstb.1998.0281.
Hyvärinen, A., Oja, E., 2000. Independent component analysis: algorithms and applications. Neural Netw 13, 411–430. doi:10.1016/S0893-6080(00)00026-5.
Jensen, O., Colgin, L.L., 2007. Cross-frequency coupling between neuronal oscillations. Trends Cogn. Sci. 11, 267–269. doi:10.1016/j.tics.2007.05.003.
Jensen, O., Mazaheri, A., 2010. Shaping Functional Architecture by Oscillatory Alpha Activity: Gating by Inhibition. Front. Hum. Neurosci. 4. doi:10.3389/fnhum.2010.00186.
Ju, H., Bassett, D.S., 2020. Dynamic representations in networked neural systems. Nat. Neurosci. 23, 908–917. doi:10.1038/s41593-020-0653-3.
Kastner, S., Ungerleider, L.G., 2000. Mechanisms of Visual Attention in the Human Cortex. Annu. Rev. Neurosci. 23, 315–341. doi:10.1146/annurev.neuro.23.1.315.
Kelly, S.P., Lalor, E.C., Reilly, R.B., Foxe, J.J., 2006. Increases in Alpha Oscillatory Power Reflect an Active Retinotopic Mechanism for Distracter Suppression During Sustained Visuospatial Attention. J. Neurophysiol. 95, 3844–3851. doi:10.1152/jn.01234.2005.
Ki, J.J., Kelly, S.P., Parra, L.C., 2016. Attention Strongly Modulates Reliability of Neural Responses to Naturalistic Narrative Stimuli. J. Neurosci. 36, 3092–3101. doi:10.1523/JNEUROSCI.2942-15.2016.
Klimesch, W., Doppelmayr, M.M., Wimmer, H., Gruber, W.R., Röhm, D., Schwaiger, J., Hutzler, F., 2001. Alpha and beta band power changes in normal and dyslexic children. Clin. Neurophysiol. 112, 1186–1195. doi:10.1016/S1388-2457(01)00543-0.
Klimesch, W., Sauseng, P., Hanslmayr, S., 2007. EEG alpha oscillations: The inhibition–timing hypothesis. Brain Res. Rev. 53, 63–88. doi:10.1016/j.brainresrev.2006.06.003.
Ko, L.-.W., Komarov, O., Hairston, W.D., Jung, T.-.P., Lin, C.-.T., 2017. Sustained Attention in Real Classroom Settings: An EEG Study. Front. Hum. Neurosci. 11, 388. doi:10.3389/fnhum.2017.00388.
Koelewijn, L., Dumont, J.R., Muthukumaraswamy, S.D., Rich, A.N., Singh, K.D., 2011. Induced and evoked neural correlates of orientation selectivity in human visual cortex. Neuroimage 54, 2983–2993. doi:10.1016/j.neuroimage.2010.11.045.
Kopell, N., Ermentrout, G.B., Whittington, M.A., Traub, R.D., 2000. Gamma rhythms and beta rhythms have different synchronization properties. Proc. Natl. Acad. Sci. 97, 1867–1872. doi:10.1073/pnas.97.4.1867.
Lachaux, J.-.P., Rodriguez, E., Martinerie, J., Varela, F.J., 1999. Measuring phase synchrony in brain signals. Hum. Brain Mapp. 8, 194–208. doi:10.1002/(SICI)1097-0193(1999)8:4<194::AID-HBM4>3.0.CO;2-C.
Lalo, E., Gilbertson, T., Doyle, L., Di Lazzaro, .V.., Cioni, B., Brown, P., 2007. Phasic increases in cortical beta activity are associated with alterations in sensory processing in the human. Exp. Brain Res. 177, 146. doi:10.1007/s00221-006-0828-5, 146.
Latora, V., Marchiori, M., 2001. Efficient Behavior of Small-World Networks. Phys. Rev. Lett. 87, 198701. doi:10.1103/PhysRevLett.87.198701.
Lehmann, D., Skrandies, W., 1980. Reference-free identification of components of checkerboard-evoked multichannel potential fields. Electroencephalogr. Clin. Neurophysiol. 48, 609–621. doi:10.1016/0013-4694(80)90419-8.
Lundqvist, M., Rose, J., Herman, P., Brincat, S.L., Buschman, T.J., Miller, E.K., 2016. Gamma and beta bursts underlie working memory. Neuron 90, 152–164.
Maris, E., Oostenveld, R., 2007. Nonparametric statistical testing of EEG- and MEG-data. J. Neurosci. Methods 164, 177–190. doi:10.1016/j.jneumeth.2007.03.024.
Martínez-Cancino, R., Heng, J., Delorme, A., Kreutz-Delgado, K., Sotero, R.C., Makeig, S., 2019. Measuring transient phase-amplitude coupling using local mutual information. Neuroimage 185, 361–378. doi:10.1016/j.neuroimage.2018.10.034.
Mathewson, K.E., Lleras, A., Beck, D.M., Fabiani, M., Ro, T., Gratton, G., 2011. Pulsed Out of Awareness: EEG Alpha Oscillations Represent a Pulsed-Inhibition of Ongoing Cortical Processing. Front. Psychol. 2. doi:10.3389/fpsyg.2011.00099.
Mazaheri, A., Jensen, O., 2010. Rhythmic pulsing: linking ongoing brain activity with evoked responses. Front. Hum. Neurosci. 4. doi:10.3389/fnhum.2010.00177.
Mazaheri, A., Picton, T.W., 2005. EEG spectral dynamics during discrimination of auditory and visual targets. Cogn. Brain Res. 24, 81–96. doi:10.1016/j.cogbrainres.2004.12.013.
Michel, C.M., Murray, M.M., Lantz, G., Gonzalez, S., Spinelli, L., Grave de Peralta, R., 2004. EEG source imaging. Clin. Neurophysiol 115, 2195–2222. doi:10.1016/j.clinph.2004.06.001.
Milde, T., Leistritz, L., Astolfi, L., Miltner, W.H., Weiss, T., Babiloni, F., Witte, H., 2010. A new Kalman filter approach for the estimation of high-dimensional time-variant multivariate AR models and its application in analysis of laser-evoked brain potentials. Neuroimage 50, 960–969. doi:10.1016/j.neuroimage.2009.12.110.
Minami, T., Noritake, Y., Nakauchi, S., 2014. Decreased beta-band activity is correlated with disambiguation of hidden figures. Neuropsychologia 56, 9–16. doi:10.1016/j.neuropsychologia.2013.12.026.
Noonan, M.P., Adamian, N., Pike, A., Printzlau, F., Crittenden, B.M., Stokes, M.G., 2016. Distinct Mechanisms for Distractor Suppression and Target Facilitation. J. Neurosci. 36, 1797–1807. doi:10.1523/JNEUROSCI.2133-15.2016.
Oliveira, F.T.P., Hickey, C., McDonald, J.J., 2014. Proactive and Reactive Processes in the Medial Frontal Cortex: An Electrophysiological Study. PLoS ONE 9, e84351. doi:10.1371/journal.pone.0084351.
Oostenveld, R., Fries, P., Maris, E., Schoffelen, J.-.M., 2011. FieldTrip: Open Source Software for Advanced Analysis of MEG, EEG, and Invasive Electrophysiological Data. Comput. Intell. Neurosci. 2011, 1–9. doi:10.1155/2011/156869.
Pagnotta, M.F., Dhamala, M., Plomp, G., 2018a. Assessing the performance of Granger–Geweke causality: Benchmark dataset and simulation framework. Data Brief 21, 833–851. doi:10.1016/j.dib.2018.10.034.
Pagnotta, M.F., Dhamala, M., Plomp, G., 2018b. Benchmarking nonparametric Granger causality: Robustness against downsampling and influence of spectral decomposition parameters. Neuroimage 183, 478–494. doi:10.1016/j.neuroimage.2018.07.046.
Pagnotta, M.F., Plomp, G., 2018. Time-varying MVAR algorithms for directed connectivity analysis: Critical comparison in simulations and benchmark EEG data. PLoS ONE 13, e0198846. doi:10.1371/journal.pone.0198846.
Pascual-Marqui, R., Biscay, R.J., Bosch-Bayard, J., Faber, P., Kinoshita, T., Kochi, K., Milz, P., Nishida, K., Yoshimura, M., 2017. Innovations orthogonalization: a solution to the major pitfalls of EEG/MEG "leakage correction." 10.1101/178657
Pascucci, D., Hervais-Adelman, A., Plomp, G., 2018. Gating by induced A-Γ asynchrony in selective attention. Hum. Brain Mapp. 39, 3854–3870. doi:10.1002/hbm.24216.
Pascucci, D., Rubega, M., Plomp, G., 2020. Modeling time-varying brain networks with a self-tuning optimized Kalman filter. PLOS Comput. Biol. 16, e1007566. doi:10.1371/journal.pcbi.1007566.
Peirce, J., Gray, J.R., Simpson, S., MacAskill, M., Höchenberger, R., Sogo, H., Kastman, E., Lindeløv, J.K., 2019. PsychoPy2: Experiments in behavior made easy. Behav. Res. Methods 51, 195–203. doi:10.3758/s13428-018-01193-y.
Penny, W.D., Duzel, E., Miller, K.J., Ojemann, J.G., 2008. Testing for nested oscillation. J. Neurosci. Methods 174, 50–61. doi:10.1016/j.jneumeth.2008.06.035.
Perrin, F., Pernier, J., Bertrand, O., Echallier, J.F., 1989. Spherical splines for scalp potential and current density mapping. Electroencephalogr. Clin. Neurophysiol. 72, 184–187. doi:10.1016/0013-4694(89)90180-6.
Pfurtscheller, G., Lopes da Silva, F.H., 1999. Event-related EEG/MEG synchronization and desynchronization: basic principles. Clin. Neurophysiol. 110, 1842–1857. doi:10.1016/S1388-2457(99)00141-8.
Pfurtscheller, G., Stancák, A.A., Neuper, C., 1996. Post-movement beta synchronization. A correlate of an idling motor area? Electroencephalogr. Clin. Neurophysiol. 98, 281–293. doi:10.1016/0013-4694(95)00258-8.
Pogosyan, A., Gaynor, L.D., Eusebio, A., Brown, P., 2009. Boosting Cortical Activity at Beta-Band Frequencies Slows Movement in Humans. Curr. Biol. 19, 1637–1641. doi:10.1016/j.cub.2009.07.074.
Popov, T., Kastner, S., Jensen, O., 2017. FEF-Controlled Alpha Delay Activity Precedes Stimulus-Induced Gamma-Band Activity in Visual Cortex. J. Neurosci. 37, 4117–4127. doi:10.1523/JNEUROSCI.3015-16.2017.
Poulsen, A.T., Kamronn, S., Dmochowski, J., Parra, L.C., Hansen, L.K., 2017. EEG in the classroom: Synchronised neural recordings during video presentation. Sci. Rep. 7, 43916. doi:10.1038/srep43916.
Richter, C.G., Coppola, R., Bressler, S.L., 2018. Top-down beta oscillatory signaling conveys behavioral context in early visual cortex. Sci. Rep. 8. doi:10.1038/s41598-018-25267-1.
Richter, C.G., Thompson, W.H., Bosman, C.A., Fries, P., 2017. Top-Down Beta Enhances Bottom-Up Gamma. J. Neurosci 37, 6698–6711. doi:10.1523/JNEUROSCI.3771-16.2017.
Riddle, J., Hwang, K., Cellier, D., Dhanani, S., D'Esposito, M., 2019. Causal Evidence for the Role of Neuronal Oscillations in Top–Down and Bottom–Up Attention. J. Cogn. Neurosci. 1–12. doi:10.1162/jocn_a_01376.
Rubega, M., Carboni, M., Seeber, M., Pascucci, D., Tourbier, S., Toscano, G., Van Mierlo, P., Hagmann, P., Plomp, G., Vulliemoz, S., Michel, C.M., 2019. Estimating EEG Source Dipole Orientation Based on Singular-value Decomposition for Connectivity Analysis. Brain Topogr. doi:10.1007/s10548-018-0691-2.
Rubinov, M., Sporns, O., 2010. Complex network measures of brain connectivity: Uses and interpretations. Neuroimage 52, 1059–1069. doi:10.1016/j.neuroimage.2009.10.003.
Saalmann, Y.B., Pinsk, M.A., Wang, L., Li, X., Kastner, S., 2012. The Pulvinar Regulates Information Transmission Between Cortical Areas Based on Attention Demands. Science 337, 753–756. doi:10.1126/science.1223082.
Sanes, J.N., Donoghue, J.P., 1993. Oscillations in local field potentials of the primate motor cortex during voluntary movement. Proc. Natl. Acad. Sci. 90, 4470–4474. doi:10.1073/pnas.90.10.4470.
Schmiedt, J.T., Maier, A., Fries, P., Saunders, R.C., Leopold, D.A., Schmid, M.C., 2014. Beta Oscillation Dynamics in Extrastriate Cortex after Removal of Primary Visual Cortex. J. Neurosci. 34, 11857–11864. doi:10.1523/JNEUROSCI.0509-14.2014.
Schneider, S.L., Rose, M., 2016. Intention to encode boosts memory-related pre-stimulus EEG beta power. Neuroimage 125, 978–987. doi:10.1016/j.neuroimage.2015.11.024.
Schoenfeld, M.A., Hopf, J.-.M., Martinez, A., Mai, H., Sattler, C., Gasde, A., Heinze, H.-.J., Hillyard, S.A., 2007. Spatio-temporal Analysis of Feature-Based Attention. Cereb. Cortex 17, 2468–2477. doi:10.1093/cercor/bhl154.
Schroeder, S.C.Y., Ball, F., Busch, N.A., 2018. The role of alpha oscillations in dis-

tractor inhibition during memory retention. Eur. J. Neurosci. 48, 2516–2526. doi:10.1111/ejn.13852.
Scolari, M., Ester, E.F., Serences, J.T., 2014. Feature- and Object-Based Attentional Modulation in the Human Visual System. Oxford University Press doi:10.1093/oxfordhb/9780199675111.013.009.
Seeber, M., Cantonas, L.-.M., Hoevels, M., Sesia, T., Visser-Vandewalle, V., Michel, C.M., 2019. Subcortical electrophysiological activity is detectable with high-density EEG source imaging. Nat. Commun. 10, 753. doi:10.1038/s41467-019-08725-w.
Serences, J.T., Yantis, S., 2007. Spatially Selective Representations of Voluntary and Stimulus-Driven Attentional Priority in Human Occipital, Parietal, and Frontal Cortex. Cereb. Cortex 17, 284–293. doi:10.1093/cercor/bhj146.
Seth, A.K., Barrett, A.B., Barnett, L., 2015. Granger Causality Analysis in Neuroscience and Neuroimaging. J. Neurosci. 35, 3293–3297. doi:10.1523/JNEUROSCI.4399-14.2015.
Siegel, M., Warden, M.R., Miller, E.K., 2009. Phase-dependent neuronal coding of objects in short-term memory. Proc. Natl. Acad. Sci. 106, 21341–21346. doi:10.1073/pnas.0908193106.
Simoncelli, E.P., Olshausen, B.A., 2001. Natural Image Statistics and Neural Representation. Annu. Rev. Neurosci. 24, 1193–1216. doi:10.1146/annurev.neuro.24.1.1193.
Snyder, A.C., Foxe, J.J., 2010. Anticipatory attentional suppression of visual features indexed by oscillatory alpha-band power increases: a high-density electrical mapping study. J. Neurosci. 30, 4024–4032.
Sperdin, H.F., Coito, A., Kojovic, N., Rihs, T.A., Jan, R.K., Franchini, M., Plomp, G., Vulliemoz, S., Eliez, S., Michel, C.M., Schaer, M., 2018. Early alterations of social brain networks in young children with autism. Elife 7, e31670. doi:10.7554/eLife.31670.
Spitzer, B., Haegens, S., 2017. Beyond the Status Quo: A Role for Beta Oscillations in Endogenous Content (*Re*)Activation. eNeuro 4. doi:10.1523/ENEURO.0170-17.2017, ENEURO.0170-17.2017.
Swann, N., Tandon, N., Canolty, R., Ellmore, T.M., McEvoy, L.K., Dreyer, S., DiSano, M., Aron, A.R., 2009. Intracranial EEG Reveals a Time- and Frequency-Specific Role for the Right Inferior Frontal Gyrus and Primary Motor Cortex in Stopping Initiated Responses. J. Neurosci. 29, 12675–12685. doi:10.1523/JNEUROSCI.3359-09.2009.
Takahashi, D.Y., Baccalá, L.A., Sameshima, K., 2010. Information theoretic interpretation of frequency domain connectivity measures. Biol. Cybern. 103, 463–469. doi:10.1007/s00422-010-0410-x.
Toppi, J., Babiloni, F., Vecchiato, G., De Vico Fallani, F., Mattia, D., Salinari, S., Bolton, T.A., Leistritz, L., Witte, H., Astolfi, L., 2012. Towards the time varying estimation of complex brain connectivity networks by means of a General Linear Kalman Filter approach, in: engineering in Medicine and Biology Society (EMBC). In: 2012 Annual International Conference of the IEEE. IEEE, pp. 6192–6195. doi:10.1109/EMBC.2012.6347408.
Torrence, C., Compo, G.P., 1998. A Practical Guide to Wavelet Analysis. Bull. Am. Meteorol. Soc. 79, 61–78. doi:10.1175/1520-0477(1998)079<0061:APGTWA>2.0.CO;2.
Tort, A.B.L., Komorowski, R., Eichenbaum, H., Kopell, N., 2010. Measuring Phase-Amplitude Coupling Between Neuronal Oscillations of Different Frequencies. J. Neurophysiol. 104, 1195–1210. doi:10.1152/jn.00106.2010.
Van de Steen, F., Faes, L., Karahan, E., Songsiri, J., Valdes-Sosa, P.A., Marinazzo, D., 2016. Critical Comments on EEG Sensor Space Dynamical Connectivity Analysis. Brain Topogr. doi:10.1007/s10548-016-0538-7.
Van Diepen, R.M., Foxe, J.J., Mazaheri, A., 2019. The functional role of alpha-band activity in attentional processing: The current zeitgeist and future outlook. Curr. Opin. Psychol. doi:10.1016/j.copsyc.2019.03.015.
van Diepen, R.M., Mazaheri, A., 2017. Cross-sensory modulation of alpha oscillatory activity: suppression, idling, and default resource allocation. Eur. J. Neurosci. 45, 1431–1438. doi:10.1111/ejn.13570.
Van Veen, B.D., Van Drongelen, W., Yuchtman, M., Suzuki, A., 1997. Localization of brain electrical activity via linearly constrained minimum variance spatial filtering. IEEE Trans. Biomed. Eng. 44, 867–880. doi:10.1109/10.623056.
von Stein, A., Sarnthein, J., 2000. Different frequencies for different scales of cortical integration: from local gamma to long range alpha/theta synchronization. Int. J. Psychophysiol. 38, 301–313. doi:10.1016/S0167-8760(00)00172-0.
Voytek, B., Canolty, R.T., Shestyuk, A., Crone, N., Parvizi, J., Knight, R.T., 2010. Shifts in gamma phase–amplitude coupling frequency from theta to alpha over posterior cortex during visual tasks. Front. Hum. Neurosci. 4. doi:10.3389/fnhum.2010.00191.
Voytek, B., D'Esposito, M., Crone, N., Knight, R.T., 2013. A method for event-related phase/amplitude coupling. Neuroimage 64, 416–424. doi:10.1016/j.neuroimage.2012.09.023.
Watson, A.B., Pelli, D.G., 1983. Quest: A Bayesian adaptive psychometric method. Percept. Psychophys. 33, 113–120. doi:10.3758/BF03202828.
Watts, D.J., Strogatz, S.H., 1998. Collective dynamics of 'small-world' networks. Nature 393, 440–442. doi:10.1038/30918.
Worden, M.S., Foxe, J.J., Wang, N., Simpson, G.V., 2000. Anticipatory Biasing of Visuospatial Attention Indexed by Retinotopically Specific α-Bank Electroencephalography Increases over Occipital Cortex. J. Neurosci. 20, RC63. doi:10.1523/JNEUROSCI.20-06-j0002.2000, RC63.
Yordanova, J., Kolev, V., Polich, J., 2001. P300 and alpha event-related desynchronization (ERD). Psychophysiology 38, 143–152. doi:10.1111/1469-8986.3810143.